SEIS**M**ICA

Comparison of geodetic slip-deficit and geologic fault slip rates reveals that variability of elastic strain accumulation and release rates on strike-slip faults is controlled by the relative structural complexity of plate-boundary fault systems

J. Gauriau (ID) * [1], J.F. Dolan (ID) [1]

[1] Department of Earth Sciences, University of Southern California, Los Angeles, CA, USA

Author contributions: *Conceptualization*: J. Gauriau, J. F. Dolan. *Data Curation*: J. Gauriau. *Formal Analysis*: J. Gauriau. *Investigation*: J. Gauriau. *Methodology*: J. Gauriau. *Project Administration*: J. Gauriau. *Resources*: J. Gauriau, J. F. Dolan. *Software*: J. Gauriau. *Supervision*: J. F. Dolan. *Validation*: J. F. Dolan. *Visualization*: J. Gauriau. *Writing – original draft*: J. Gauriau. *Writing – review & editing*: J. F. Dolan, J. Gauriau.

Abstract   Comparison of geodetic slip-deficit rates with geologic fault slip rates on major strike-slip faults reveals marked differences in patterns of elastic strain accumulation on tectonically isolated faults relative to faults that are embedded within more complex plate-boundary fault systems. Specifically, we show that faults that extend through tectonically complex systems characterized by multiple, mechanically complementary faults (that is, different faults that are all accommodating the same deformation field), which we refer to as high-Coefficient of Complexity (or high-CoCo) faults, exhibit ratios between geodetic and geologic rates that vary and that depend on the displacement scales over which the geologic slip rates are averaged. This indicates that elastic strain accumulation rates on these faults change significantly through time, which in turn suggests that the rates of ductile shear beneath the seismogenic portion of faults also vary through time. This is consistent with models in which mechanically complementary faults trade off slip in time and space in response to varying mechanical and stress conditions on the different component faults. In marked contrast, structurally isolated (or low-CoCo) faults exhibit geologic slip rates that are similar to geodetic slip-deficit rates, regardless of the displacement and time scales over which the slip rates are averaged. Such faults experience relatively constant geologic fault slip rates as well as constant strain accumulation rate (aside from brief, rapid post-seismic intervals). This suggests that low-CoCo faults "keep up" with the rate imposed by the relative plate-boundary condition, since they are the only structures in their respective plate-boundary zone that can effectively accommodate the imposed steady plate motion. We hypothesize that the discrepancies between the small-displacement average geologic slip rates and geodetic slip-deficit rates may provide a means of assessing a switch of modes for some high-CoCo faults, transitioning from a slow mode to a faster mode, or vice versa. If so, the differences between geologic slip rates and geodetic slip-deficit rates on high-CoCo faults may indicate changes in a fault's behavior that could be used to refine next-generation probabilistic seismic hazard assessments.

Non-technical summary   Geodetic slip-deficit rates record how much elastic strain energy accumulates along a fault, whereas geologic slip rates record the actual slip that occurred throughout multiple earthquakes along that fault during release of the stored elastic strain energy. We look at multiple active faults within strike-slip plate boundary fault systems, and compare geodetic slip-deficit rates with geologic slip rates averaged over different fault displacement scales. We find that these values tend to be similar for isolated faults at all scales, whereas they differ in structurally complex fault systems. We conclude that both the accumulation and release of elastic strain energy is constant on faults embedded in simple settings, but varies in complex fault systems.

1   Introduction

Unravelling the relationship between geologic fault slip rates and rates of strain accumulation as measured by geodesy is critically important for developing a better understanding of the mechanics of faults and the seismic hazards that they pose. Whereas some major faults exhibit constant behavior, with relatively steady geologic slip rates spanning a range of time and displacement scales (e.g., Kozacı et al., 2009, 2011; Berryman et al., 2012; Salisbury et al., 2018; Grant Ludwig et al., 2019), other faults exhibit highly irregular slip rates through time, with centennial to millennial periods of relatively fast slip rate spanning multiple earthquake cycles, separated by prolonged periods of slower or no slip rate (e.g., Benedetti et al., 2002; Friedrich et al., 2003;

*Corresponding author: gauriau@usc.edu

Bull et al., 2006; Dolan et al., 2016; Hatem et al., 2020; Zinke et al., 2017, 2019, 2021).

Elastic strain accumulation rates inferred from analysis of geodetic data reflect the shearing velocity of the seismogenic faults' underlying ductile roots, and have been suggested to be relatively constant beyond the single-earthquake scale (i.e., once fast post-seismic and slower interseismic rates have been averaged out). Indeed, comparisons of geodetic slip-deficit and geologic rates have been used to infer near-constant interseismic rates. For example, in one of the largest such compilations to date, Meade et al. (2013) compared geologic fault slip rates and geodetic slip-deficit rates for 15 major continental strike-slip faults around the world. Their results suggest that, as an ensemble, these faults exhibit a near 1:1 relationship (with a slope of 0.94 ± 0.09) between geologic and geodetic rates. Slight differences between the datasets could be attributable to short-lived periods of higher-than-average strain accumulation during the post-seismic period. The geologic rates used as inputs into the analysis of Meade et al. (2013) span a huge range of displacement and time scales, from as small as ~13 m to as large as ~600 m, and as short as 2 ky to as long as 160 ky. We recently presented results that demonstrate that, for faults that lie within complex plate-boundary fault networks, geologic slip rates vary depending on the displacement scale over which the slip rate is estimated; on the other hand, structurally isolated faults that accommodate most of the relative motion within simple plate boundaries exhibit steadier slip rates (Gauriau and Dolan, 2021). These observations lead us to explore the possibility that differences between geodetic slip-deficit rates and geologic slip rates might also be sensitive to the relative complexity of the surrounding fault network. If they are, this would require that geodetic-geologic rate comparisons consider time and displacement scales over which incremental slip rates are averaged, as well as the relative structural complexity of the surrounding fault system, especially in structurally complex plate boundaries (e.g., northern and southern California, Marlborough fault system in New Zealand), that are characterized by multiple, mechanically complementary faults.

In this paper, we explore the potential constancy, or lack thereof, of the elastic strain accumulation rate patterns on active strike-slip faults. Specifically, we aim to investigate the relative constancy and potential variability of elastic strain accumulation rates on faults characterized by temporally constant geologic slip rates, on the one hand, and faults that exhibit temporally variable geologic slip rates, on the other. Comparing elastic strain accumulation rates derived from geodesy with geologic slip rates has been done in several studies (e.g., Kozacı et al., 2009; Meade et al., 2013; Tong et al., 2014; Dolan and Meade, 2017; Evans et al., 2016) but never in light of the relative complexity of the plate-boundary fault systems being considered.

2 Studied faults and terminology

In this study, we use the recently developed Coefficient of Complexity (CoCo) method (Gauriau and Dolan,

2021), which quantifies the relative structural complexity of the fault network surrounding a fault of interest by integrating the density and displacement rates of the faults in the plate-boundary network at a specific radius (here, 100 km) around the site of interest. The method is illustrated in Figure 1. We use CoCo values calculated for 18 major strike-slip faults for which both geologic incremental slip-rate records and geodetic slip-deficit rates are available (Figure 2, Table 1). In total, we work with 24 different fault sites where these two kinds of data are available and approximately collocated. The comparison of the CoCo values for all sites is then enabled by the standardization of the CoCo values by the respective plate-motion rate, totaled for the observation area of 100 km radius. This allows direct comparisons of the intensity of fault activity in different plate-boundary fault networks that move at different relative plate motion rates.

We divide the available geologic slip-rate data into two groups: large-displacement slip rates and small-displacement slip rates (usually referred to as "long-term" and "short-term" slip rates, respectively), which are averaged over large (> ~50 m) and small (< ~50 m) displacements, respectively (Table 1). The reasons for this are twofold: (a) This allows us to discuss fast- and slow-slipping faults with comparable parameters and hence by considering similar numbers of earthquakes on faults that have widely different recurrence intervals, and (b) displacement, not time, may be what matters most in terms of the mechanisms governing fault behavior in complex plate-boundary fault systems (Dolan et al., 2007; Cawood and Dolan, submitted; Dolan et al., 2024). In addition, we use the terms "geodetic slip-deficit rates" to refer to any rate that was obtained on the basis of space geodetic measurements of surface ground displacement over multi-annual to decadal time scales, such as Global Positioning System (GPS) or Interferometric Synthetic Aperture Radar (InSAR), and which has been modeled to characterize the most recent rate of elastic strain accumulation for the studied strike-slip faults.

3 Consideration of elapsed time since most recent event relative to sampling geodetic slip-deficit rates

In order to evaluate potential differences in behavior of faults embedded within structurally simple fault systems (i.e., low-CoCo faults) versus faults embedded within structurally complex fault networks (i.e., high-CoCo faults), we compare geodetic slip-deficit rates with geologic fault slip rates that are averaged over both small displacements and large displacements. We first introduce a few key considerations that allow us to carry out this comparison between geodetic and geologic data.

The interseismic geodetic data used in this paper may derive from different sampling times throughout the earthquake cycle. Although we have no precise control over where exactly the examined faults lie in their elastic strain cycles, we can in most instances document the elapsed time since their most recent event (MRE),

Fault	Section/ Site	#	SD slip rate (mm/yr)	Time range of SD slip rate (ky)	Displace-ment of SD slip rate (m)	References for SD slip rate	LD slip rate (mm/yr)	Time range of LD slip rate (ky)	Displace-ment of LD slip rate (m)	References for LD slip rate	Geodetic rate (mm/yr)	References for geodetic rate	Plate rate (mm/yr)	References
Garlock	Central	1	$14^{+2.2}_{-1.8}$	1.9	$26^{+3.5}_{-2.5}$	(Dolan et al., 2016)	8.8 ± 1.0	8.0 ± 0.9	70 ± 7	(Fougere et al., 2023)	2.61 ± 3.00	(Evans, 2017b)	49	(Dolan et al., 2016); (McGill and Sieh, 1993; Evans, 2017a)
San Andreas	Mojave	2	$28.8^{+1.5}_{-0.8}$	$1.007^{+0.028}_{-0.050}$	~29	(Weldon et al., 2004; Dolan et al., 2016)	$30.9^{+2.9}_{-2.5}$	1.49 ± 0.13	46	(Weldon et al., 2004)	15.12 ± 2.78		49	(Weldon et al., 2004; Dolan et al., 2016; Evans, 2017a)
	Carrizo Plain	3	$31.6^{+9.0}_{-6.6}$	0.38 ± 0.06	12 ± 1	(Salisbury et al., 2018)	36 ± 1	~3.5	128 ± 1	Grant-Ludwig et al. (2019)	35.65 ± 5.11		39	(Grant Ludwig et al., 2019; Salisbury et al., 2018; Sieh and Jahns, 1984; Noriega et al., 2006)
San Jacinto	Clare-mont	4	12.8 - 18.3	2.05 ± 0.12	25 - 30	(Onderdonk et al., 2015)					13.18 ± 4.61		49	(Onderdonk et al., 2015; Evans, 2017b)
Owens Valley		5	0.5-2.1 [§]			(Haddon et al., 2016) and refer-ences therein	2.8-4.5	55-80	235 ± 15	(Kirby et al., 2008)	2.71 ± 1.38		12	(Kirby et al., 2008; Haddon et al., 2016; Evans, 2017a)
Calico	Central	6					1.6 ± 0.2	650 ± 100	900 ± 200	(Oskin et al., 2007)	7.42 ± 3.44		49	(Oskin et al., 2004, 2008; Evans, 2017a)
Hope	Conway	7	$8.2^{+5.4}_{-3.0}$	ca. 1.1	12 ± 2	(Hatem et al., 2020)	$15.2^{+2.2}_{-2.4}$	ca. 13.8	210 ± 15	(Hatem et al., 2020)	$5.8^{+1.8}_{-1.1}$	(Johnson et al., 2022)	39	(Hatem et al., 2020; Johnson et al., 2022)
Wairau	Branch River Dunbeath	8	4.5 ± 1.0 [*]	3.3 ± 0.4	15 ± 2.6	(Zinke et al., 2021)	4.9 ± 0.4	$11.9^{+1.0}_{-0.8}$	58.5 ± 2	(Zinke et al., 2021)	$2.8^{+2.4}_{-0.8}$			(Zinke et al., 2021; Johnson et al., 2022)
Clarence	Tophouse Road	9	2.0 ± 0.4	$4.5^{+0.8}_{-0.7}$	9.0 ± 1.0	(Zinke et al., 2019)	4.2 ± 0.5	11.2 ± 1.3	47.0 ± 3.0	(Zinke et al., 2019)	$8.6^{+1.4}_{-1.1}$			(Zinke et al., 2019; Johnson et al., 2022)
Awatere	Saxton River	10	$4.2^{+1.2}_{-1.0}$	1.8 ± 0.3	9.5 ± 1.0	(Zinke et al., 2017)	$5.6^{+0.8}_{-0.6}$	$12.9^{+1.2}_{-1.0}$	72.5 ± 7.5	(Zinke et al., 2017)	$1.9^{+2.2}_{-0.8}$			(Zinke et al., 2017; Johnson et al., 2022)
Alpine	Southern	11					$29.6^{+4.5}_{-2.5}$	270	8000	(Barth et al., 2014)	$29.1^{+1.1}_{-3.2}$			(Berryman et al., 2012; Page et al., 2018; Wallace et al., 2012)

Table 1 Continued on next page

Fault	Section/Site	#	SD slip rate (mm/yr)	Time range of SD slip rate (ky)	Displacement of SD slip rate (m)	References for SD slip rate	LD slip rate (mm/yr)	Time range of LD slip rate (ky)	Displacement of LD slip rate (m)	References for LD slip rate	Geodetic rate (mm/yr)	References for geodetic rate	Plate rate (mm/yr)	References
Dead Sea	Wadi Araba Valley	12	3.8 - 6.1	2 - 4.2	13.2 ± 1.0	(Klinger et al., 2000)	4 ± 2	140 ± 31	300-900	(Klinger et al., 2000)	5.0 ± 0.2	(Gomez et al., 2020)	7	(Klinger et al., 2000; Niemi et al., 2001; Hamiel et al., 2018)
	Beteiha	13	3.5 ± 0.2 [$]	1.472	5.2 ± 0.3	(Wechsler et al., 2018)					4.8 ± 0.3			(Wechsler et al., 2018; Masson et al., 2015)
Yam-mouneh		14	3.5 - 7.5	6 - 10	40 ± 5	(Daëron et al., 2004)	2.7-7.3	12 - 27	80 ± 8	(Daëron et al., 2004)	2.5 ± 0.5			(Daëron et al., 2004; Gomez et al., 2003, 2007)
Queen Charlotte		15					52.9 ± 3.2	17 ± 0.7	900 ± 40	(Brothers et al., 2020)	46.3 ± 0.6	(Elliott and Freymueller, 2020)	55	(Brothers et al., 2020; Elliott and Freymueller, 2020)
Denali	Central	16					12.1 ± 1.7	12.0 ± 1.3 / 11.9 ± 1.3 [#]	144 ± 14	(Matmon et al., 2006)	7.0 ± 0.3		17	(Matmon et al., 2006; Elliott and Freymueller, 2020; Bender et al., 2023)
	Western	17	10.4 ± 3.0	2.4 ± 0.3	$25 \, ^{+5}_{-7}$	(Matmon et al., 2006)	9.4 ± 1.6	16.8 ± 1.8	158 ± 14	(Matmon et al., 2006)	7.75 ± 0.3		17	(Matmon et al., 2006; Elliott and Freymueller, 2020; Bender et al., 2023)

Table 1   Continued on next page

Fault	Section/Site	#	SD slip rate (mm/yr)	Time range of SD slip rate (ky)	Displacement of SD slip rate (m)	References for SD slip rate	LD slip rate (mm/yr)	Time range of LD slip rate (ky)	Displacement of LD slip rate (m)	References for LD slip rate	Geodetic rate (mm/yr)	References for geodetic rate	Plate rate (mm/yr)	References
Altyn Tagh	Central	18	9.4 ± 0.9 ¤	5.889 – 5.658	54 ± 5	(Cowgill, 2007)	9.4 ± 2.3	16.6 ± 3.9	156 ± 10	(Cowgill et al., 2009)	9 ± 4	(Bendick et al., 2000)	11.2	(Cowgill, 2007; Cowgill et al., 2009; Bendick et al., 2000; Shen et al., 2001; He et al., 2013; Zhang et al., 2007)
Kunlun	Central Western	19	10.7 ± 2.2	2.885 ± 0.285	31 ± 2	(Haibing et al., 2005)	10.6 ± 1.8	5.96 ± 0.450	63 ± 5	(Haibing et al., 2005)	11.3 ± 3.5	(Zhao et al., 2022)	12	(Van Der Woerd et al., 2002; Haibing et al., 2005; Kirby et al., 2007)
Haiyuan	Lao-hushan	20	3.7 ± 0.6	9 - 11	32 - 42	(Liu et al., 2022)	4.8 ± 0.2	15 - 17	73 - 79	(Liu et al., 2022)	$5.6 \,^{+1.3}_{-1.1}$	(Daout et al., 2016)	6.5	(Liu et al., 2018; Li et al., 2009; Shao et al., 2020)
North Anatolian	Demir Tepe Eksik	21	16.8 ± 0.1 *	0.988	15.3 ± 0.1	(Kondo et al., 2010)	20.5 ± 5.5	2 - 2.5	46 ± 10	(Kozacı et al., 2007)	20.5	(DeVries et al., 2016)	21	(Kozacı et al., 2007; Hubert-Ferrari et al., 2002)
	Tah-taköprü	22					$18.6 \,^{+3.5}_{-3.3}$	~3	55 ± 10	(Kozacı et al., 2009)	21.2 - 21.5		21	(Kozacı et al., 2009)
	Northern / Ganos	23	15 ± 6	2.5 ± 0.5	35.4 ± 1.5	(Meghraoui et al., 2012)	$18.5 \,^{+10.9}_{-5.9}$	490 ± 100	>~8000	(Kurt et al., 2013)	28.6		27	(Meghraoui et al., 2012; Kurt et al., 2013)
East Anatolian	Pazarcık, Tevekkelli	24					5.6 ± 0.3	17.8	101 ± 5	(Yönlü and Karabacak, 2023)	10.3 ± 0.6	(Aktug et al., 2016)	10	(Güvercin et al., 2022; Reilinger et al., 2006)

Table 1 Summary of data from the different fault sections used in this study, including small-displacement (SD), large-displacement (LD) averaged geologic slip rates with corresponding time and displacement ranges over which they are averaged, and geodetic slip-deficit rates. The rate values are reported as they were in their original source publications, unless specified otherwise.

* rate calculated between MRE and given offset marker

§ based on several studies cited in Haddon et al. (2016), with offsets ranging from 3 m (1 earthquake) to 19 m, and respective ages ranging from 600 years ago and 25 ka

$ averaged over the past four historical earthquakes

first age relates to boulder samples, second age refers to sediment samples (^{10}Be technique)

¤ using their upper-terrace reconstruction (Cowgill et al., 2009), as for the small-displacement slip rate

as well as an estimate of their mean earthquake recurrence interval. For a majority of the faults we study, it has been at least 100 years since the MRE, as documented historically (e.g., the 1717 Alpine fault earthquake, the 1857 Fort Tejon earthquake on the San Andreas fault, the 1872 Owens Valley earthquake) or on the basis of paleoseismological evidence (e.g., the ca. 1800-1840 CE earthquake on the Conway section of the Hope fault; Hatem et al., 2019). In a few instances, the MRE occurred more recently, such as the series of earthquakes on the North Anatolian fault between 1939 and 1999 (Barka, 1992; Barka et al., 2002), the 2002 Denali earthquake (Haeussler, 2004), or the Kahramanmaraş earthquake (e.g., Barbot et al., 2023) that occurred in Februray 2023 on the East Anatolian fault (for which we use a geodetic rate that was acquired before the earthquake).

Table S1 summarizes the MRE dates and the available mean recurrence intervals for the fault locations we study. In most of the examples, we are well into at least the middle part of the elastic strain accumulation cycle, likely well past any rapid post-seismic deformation (with the possible exceptions of the 1992 Landers, 1999 Izmit, 1999 Düzce, 1999 Hector Mine, and 2002 Denali earthquakes).

4 Relative structural complexity of the surrounding fault network in interpretation of geodetic slip-deficit rate and geologic slip-rate comparisons

In our original formulation of the CoCo metric (Gauriau and Dolan, 2021), we categorized faults as either low- or high-CoCo. To determine the CoCo metric for each fault study site, we apply a system in which we recognize that the degree of structural complexity surrounding a fault is a continuum, with no hard boundary between high- and low-CoCo faults. Whereas many of the faults we study can be readily categorized as either high-CoCo faults (e.g., the Hope fault or the Mojave section of the San Andreas fault) or low-CoCo faults (e.g., the southern Alpine fault, the central San Andreas fault), some of the faults exhibit intermediate CoCo values reflecting a surrounding plate-boundary zone that shows minor to moderate complexity. The two faults that fall in this in-between area are the Central Denali fault (16), characterized by a standardized CoCo value of $1.62 \cdot 10^{-2}$ yr^{-1} and the Altyn Tagh fault (18), characterized by a standardized CoCo value of $1.56 \cdot 10^{-2}$ yr^{-1}. Based on these two values, we use a standardized CoCo value of $1.6 \cdot 10^{-2}$ yr^{-1} as the dividing line between what we will refer to hereafter as low- and high-CoCo faults. With this boundary defined, we can explore the behaviors exhibited by these two categories of faults, as shown in Figure 2b, c (see Figure 3 for standardized CoCo values of all faults).

5 Comparison of geologic slip rates and geodetically based slip-deficit rates on strike-slip faults

Figure 2 illustrates the comparison between geologic and geodetic slip-deficit rates for the 24 different sites on the studied strike-slip faults. It reveals marked differences in the consistency of the values of the geodetic/geologic-rate pairs for high-CoCo faults relative to low-CoCo faults. Specifically, comparison of geodetic slip-deficit rates with large-displacement and small-displacement average geologic slip rates (displayed as squares and circles, respectively, in Figure 2) reveals that these rates are similar for faults characterized by low CoCo values (displayed in blue in Figure 2), whereas they differ for the faults characterized by high CoCo values (displayed in red in Figure 2). This observation is a corollary to the main conclusion of our previous study (Gauriau and Dolan, 2021), in which we showed that low-CoCo faults slip at relatively constant rates through time whereas high-CoCo faults exhibit long-term slip rates that are potentially different from the slip rates averaged over small displacements. In other words, the displacement over which the slip rate is averaged does not matter for low-CoCo faults, since any geologic slip rate will give the same value. In contrast, geologic slip rates for high-CoCo faults that are averaged over one particular displacement range may differ from the slip rate averaged over a different displacement range.

Figure 2a shows a comparison of geologic slip rates and geodetic slip-deficit rates. Figure 2b shows that low-CoCo strike-slip fault sites plot on (or near) the 1:1 line, reflecting the similarity of their short-term geodetic strain accumulation rates and both their small-displacement and large-displacement geologic strain-release rates. This can be further illustrated statistically, since the coefficient of determination obtained from an ordinary least squares regression for the low-CoCo faults is 0.983 for geologic rates averaged over large displacements, and 0.978 for geologic rates averaged over small displacements (Figure S1). Assuming a linear relationship between geologic slip rates and geodetic slip-deficit rates going through the origin, we find scaling lines with best-fit slopes and respective 1σ confidence of 0.945 ± 0.028 and 1.103 ± 0.050 for the low-CoCo faults using the large-displacement and small-displacement average geologic rates, respectively (see Figure S1a and b). These results show that for these low-CoCo faults, geodetic rates provide a reliable proxy for the geologic slip rate of the fault of interest.

That geodetic slip-deficit rates are a reliable proxy for geologic slip rate is not the case for high-CoCo faults (Figure 2c). Specifically, there is wide dispersion amongst the geodetic slip-deficit and both large- and small-displacement geologic slip rates (Figure 3). This observation requires that geodetic slip-deficit rates cannot be used as a proxy for geologic rates for high-CoCo faults, whether the rate is averaged over small displacements or large displacements. For these high-CoCo faults, the coefficient of determination obtained from an ordinary least squares regression between geologic
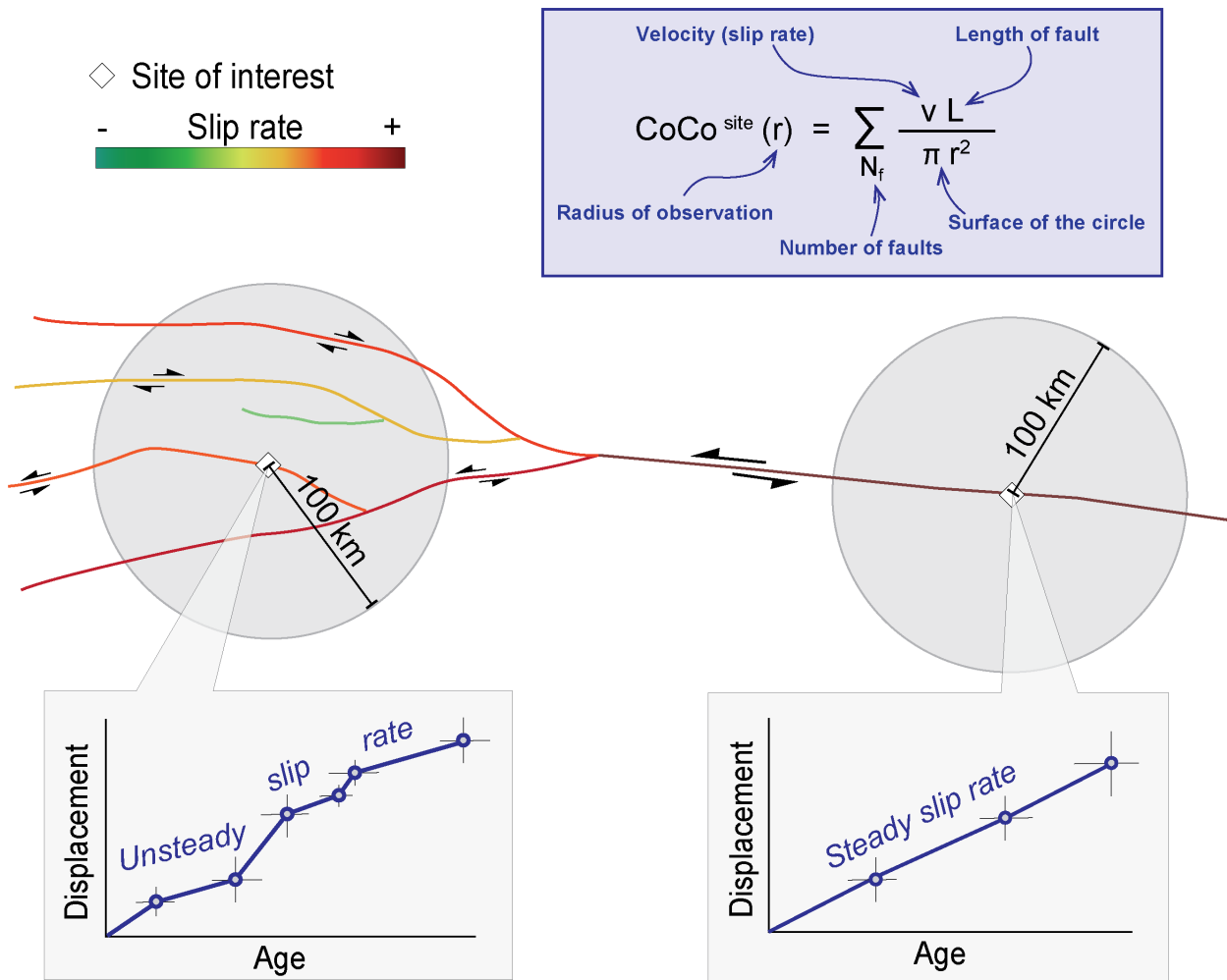
Figure 1 Schematic explanation of the rationale of the Coefficient of Complexity (CoCo) analysis for a hypothetical fault network. The calculation of CoCo for a given radius is shown on top. The radius over which CoCo is calculated is 100 km. Within a structurally complex fault system (numerous, and relatively fast-slipping faults), shown to the left, the CoCo value will be higher than within a structurally simple fault system (few or zero neighboring faults), shown to the right. The quantification of complexity, done with the CoCo analysis, correlates with the relative steadiness of geologic slip-rate record, as shown in our recent study (Gauriau and Dolan, 2021).

rates and geodetic slip-deficit rates is 0.396 for geologic rates averaged over large displacements, and 0.350 for geologic rates averaged over small displacements (Figure S1c, d). Scaling lines between geologic rates and geodetic rates for these faults, assuming a linear relationship going through the origin (as in Meade et al., 2013) are characterized by the best-fit slopes of 0.751 ± 0.162, using the small-displacement geologic rates, and 0.696 ± 0.140, using the large-displacement geologic rates (Figure S1c and d). These linear regressions seem to imply a global trend where geologic slip rates are faster than geodetic slip-deficit rates, but we suggest that these best-fit slope values are not meaningful, and are rather artifacts of the current limited state of available data. Reinforcing this idea is the observation that the dispersion of the data, shown by the standard deviations of the best-fit slopes, demonstrates that there is no good correlation between geodetic slip-deficit and geologic slip rates for high-CoCo faults. Figure 3 further illustrates this result, by displaying the ratio between the geodetic slip-deficit rates and the geologic rates averaged over large or small displacements. Figure 3b plots

a measure of distance from the data points to the 1:1 ratio line with varying CoCo values, and emphasizes the dispersion of the data for higher-CoCo faults (see details of the dispersion calculation in the Supplementary Materials); the relatively sharp increase in dispersion at standardized CoCo ~0.0015-0.002 yr^{-1} likely reflects the presence of major secondary faults that can accommodate significant portion of relative plate motions.
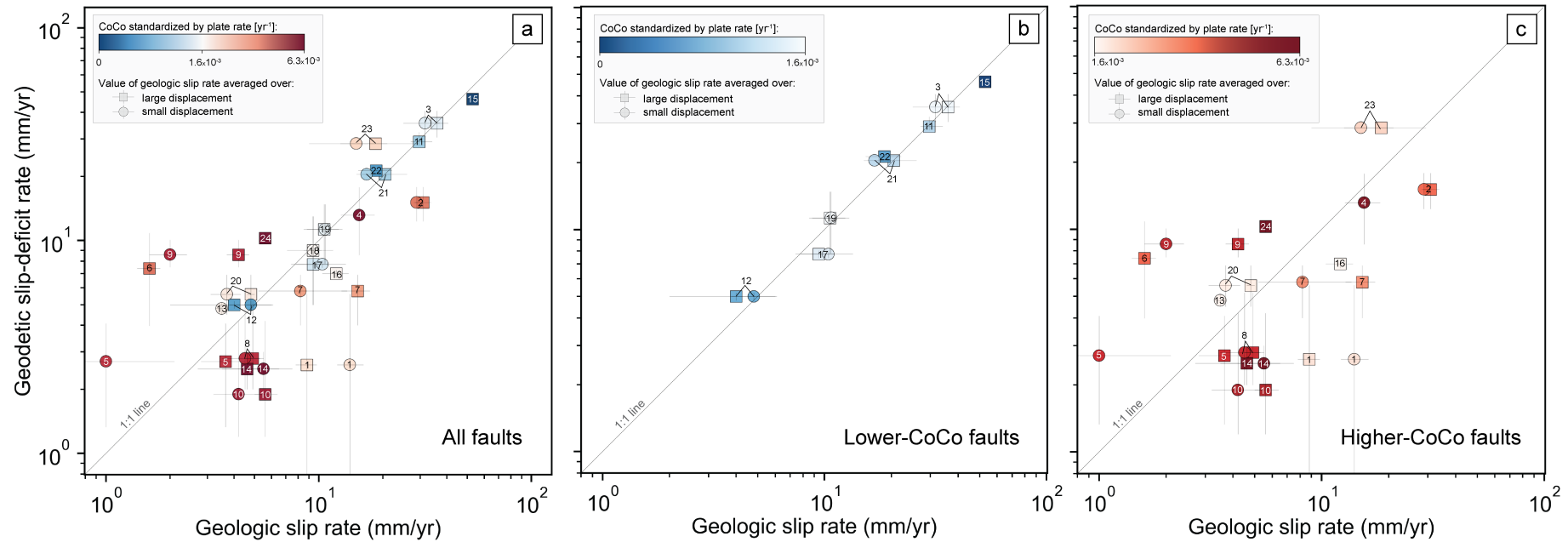
Figure 2 Geodetic slip-deficit rate and geologic slip-rate comparisons for major strike-slip faults. The geologic rates are shown as either averaged over a large displacement, or over a small displacement. The data points are color-coded according to their respective values of the Coefficient of Complexity (CoCo), standardized by the plate rate contained within a 100 km radius, as defined in Gauriau and Dolan (2021). The strike-slip faults considered in this study are: (1) Garlock, (2) San Andreas, Mojave segment, (3) San Andreas, Carrizo Plain segment, (4) San Jacinto, Claremont segment, (5) Owens Valley, (6) Calico, (7) Hope, (8) Wairau, (9) Clarence, (10) Awatere, (11) Alpine, (12) Dead Sea, Wadi Araba Valley, (13) Dead Sea, Beteiha, (14) Yammouneh, (15) Queen Charlotte, (16) Denali, central section, (17) Denali, western section, (18) Altyn Tagh, (19) Kunlun, (20) Haiyuan, (21) North Anatolian, Demir Tepe, (22) North Anatolian, Tahtaköprü, (23) Northern North Anatolian, (24) East Anatolian, Pazarcık (references listed in Table 1). **(a)** shows all the compiled faults in the same diagram. **(b)** shows all faults characterized by CoCo values that are less than 0.0016 yr^{-1} (referred to as low-CoCo faults). **(c)** shows all faults characterized by CoCo values that are more than 0.0016 yr^{-1} (referred to as high-CoCo faults).

6 Fault loading rates...

6.1 ...are constant on low-CoCo faults

Our analysis reveals that low-CoCo faults are characterized by geodetic rate/geologic rate ratios very close to one, regardless of the displacement scale over which the geologic slip rate is measured (Figures 2, 3). Geologic slip rates estimated from offset landforms at widely different displacements are the same for these faults, showing that the elastic strain release remains constant over the time intervals over which these displacements have accumulated. Furthermore, the current elastic strain accumulation rate (as constrained by the geodetic slip-deficit rate) is equal to strain release rates (as constrained by geologic slip rates) at all measured displacement scales. This indicates that for these faults, the elastic strain accumulation rate provided by the geodetic slip-deficit rate remains constant during the interseismic period (Figure 4), following the short-duration periods of fast post-seismic deformation at the beginning of each cycle, as originally noted by Meade et al. (2013).

6.2 ...vary on high-CoCo faults

In contrast, high-CoCo faults, embedded within more complex structural settings, display no consistent relationship between geodetic slip-deficit and geologic slip rates. As noted above, these results reinforce the point that geodetic slip-deficit rates cannot be used as reliable proxies for geologic slip rates on high-CoCo faults. Moreover, although the mismatch between geodetic slip-deficit rates and small-displacement geologic slip rates could conceivably be due to short-term variations in fault slip rate, the mismatch between geodetic slip-deficit rates and large-displacement geologic slip rates, which are averaged over >50 to hundreds of meters of slip (see Table 1) and numerous individual earthquakes, and will thus average over any shorter-term/smaller-displacement accelerations or decelerations of fault slip, indicates that elastic strain accumulation rates on the high-CoCo faults must vary through time. Specifically, at these large-displacement scales, the fault slip rate spanning numerous earthquakes will provide a robust estimate of the average rate of strain release on that fault through time. Insofar as the elastic strain accumulation rate must equal the elastic strain release rate (i.e., fault slip) over long time intervals, the mismatch that we document between geodetic slip-deficit rates and geologic slip rates averaged over large displacements requires that elastic strain accumulation rates as measured by geodetic slip-deficit rates must vary through time.

Further examination of the results displayed in Figure 3 helps us distinguish several types of behaviors amongst the high-CoCo faults. Those behaviors can be defined depending on whether the geodetic slip-deficit rate is equal to, slower than, or faster than either the large-displacement average geologic rate, or the small-displacement average geologic rate (Figure 4).

These differences between geodetic and geologic rates reveal the following fundamental point: Faults for which the current loading rate does not equal the average large-displacement geologic slip rate overly a ductile shear zone that must be creeping at either a slower or a faster rate than the long-term average slip rate. If, furthermore, the geodetic rate differs from the small-displacement rate, the rate of elastic strain accumulation consequently has to vary over the same periods of accelerations and decelerations that are averaged over in these small-displacement geologic rate values.

We suggest that using the mismatches between geodetic slip-deficit and small-displacement geologic rates can help us infer the current behavior of the faults that may be most representative of the near-future likelihood of major earthquake recurrence. Mismatches between elastic strain accumulation rates and small-displacement geological rates reveal three different modes for the high-CoCo faults. These are: faults that are storing elastic strain energy more slowly than their small-displacement geologic slip rates; faults that exhibit a current rate of elastic strain accumulation that is faster than the small-displacement geologic slip rate; and faults in which the geodetic slip-deficit rate approximately equals the youngest average geologic slip rate. In the following, we describe the details of the behavior of faults that fall within these three categories and discuss a model that attempts to explain the observations in terms of faults switching from one mode to another.

In the first case, geodetic slip-deficit rates are slower than the small-displacement (short-term) geologic slip rates measured on these faults. The Garlock (numbered 1 in Figures 2 and 3), the Mojave segment of the San Andreas (2), Wairau (8), Hope (9), Awatere (10), and Yammouneh (14) faults are all characterized by geodetic rate values that are slower than their respective geologic slip rates (both large- and small-displacement). For example, the central Garlock fault experienced a cluster of four large earthquakes between 0.5 and 2.0 ka (Dawson et al., 2003), resulting in a small-displacement (26 m) slip rate averaged over these four events through to the present of $14^{+2.2}_{-1.8}$ mm/yr (Dolan et al., 2016). Modeling of geodetic data consistently yields very slow rates of elastic strain accumulation on the central Garlock fault, with a best estimate of ~2.6 mm/yr (Evans, 2017b), potentially including almost no elastic strain accumulation. In contrast, the large-displacement (long-term) slip rate averaged over the most recent 70 m of slip on this section of the Garlock fault is 8.8±1.0 mm/yr (Fougere et al., 2023, submitted). While this is slower than the small-displacement geologic rate, it is at least three times faster than the current rate of elastic strain accumulation. This mismatch suggests that the Garlock fault has recently entered into a "slow" mode of elastic strain accumulation, likely as a result of a decreased shearing rate on the underlying ductile shear zone. But why is the youngest, small-displacement rate so fast? We suggest that the switch in behavior of the Garlock fault from the 0.5 – 2 ka "fast" mode ended with the final earthquake in the cluster, either because the fault (including the upper seismogenic part and the ductile shear zone roots) strengthened during the fast period encompassing the four-event cluster and became more difficult to slip (Dolan et al., 2007; Cawood and Dolan,
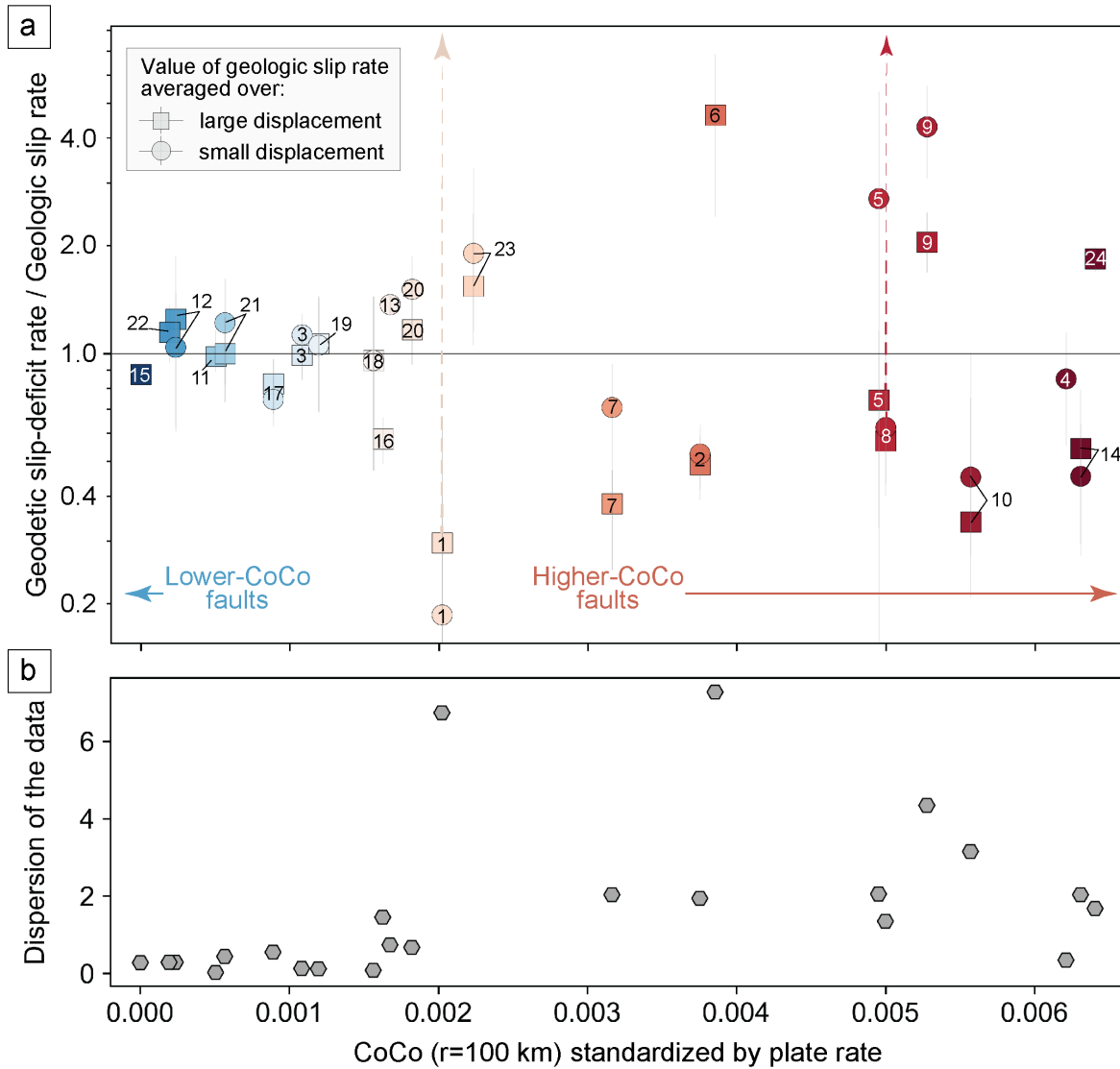
Figure 3 Variations of geodetic to geologic slip-rate ratios against CoCo values standardized by plate rate over a 100 km radius. (**a**) Ratios of geodetic slip-deficit rate to geologic rate plotted against CoCo. The geologic rate values are averaged over large or small displacement (as in Figure 2). The numbering of the fault sites is referred to in Figure 2 and Table 1. The dashed arrows refer to a ratio of geodetic/geologic rate that would reach infinity, with a geological rate close or equal to 0 mm/yr, if the fault has not slipped for a long time since the MRE (see text for details). (**b**) Diagram showing the dispersion of the ratio (geodetic to geologic rates) values varying with the CoCo values. The higher the CoCo value, the more scattered the data (i.e., the farther from the 1:1 ratio line they tend to plot). The measure of the dispersion is detailed in the Supplementary Materials. Although we cannot calculate an exact CoCo value for the Queen Charlotte fault (15), because of our inability to include all active faults within a 100 km radius of the slip-rate site, we assign it a CoCo value of zero, since this fault accommodates >95 % of the total Pacific/North America plate-motion rate (NUVEL-1A; DeMets and Dixon, 1999).

submitted), and/or because the Garlock fault has exhausted what Dolan et al. (2024) refer to as the "crustal strain capacitor" (similar to Mencin et al. (2016) "strain reservoir"), that is, the shear strain stored in the crust surrounding this section of the Garlock fault. In this view, the current slip rate (or, equivalently in this context, the "most recent geologic slip rate") of the Garlock fault since the most recent earthquake (MRE) ca. 500 years ago has been 0 mm/yr, reflecting the current very slow rate of elastic strain accumulation on the Garlock fault.

Similarly, the geodetic slip-deficit rate on the Wairau

fault in New Zealand ($2.8^{+2.4}_{-0.8}$ mm/yr; Johnson et al., 2022) is slower than the small-displacement rate of 4.5±1.0 mm/yr (Zinke et al., 2021), calculated for the preceding fast period of slip between a geomorphic offset dated at ca. 5.4 ka and the ca. 2 ka MRE. This contrast highlights a period of fast slip on the fault during this time interval. Yet, 2,000 years have elapsed since the MRE on the Wairau fault (relative to an average Holocene recurrence interval of ca. 1,000 years Nicol and Dissen, 2018), which we suggest indicates a "most recent geologic slip rate" since the MRE of 0 mm/yr. Thus, the averaging of the small-displacement rate over

High-CoCo faults
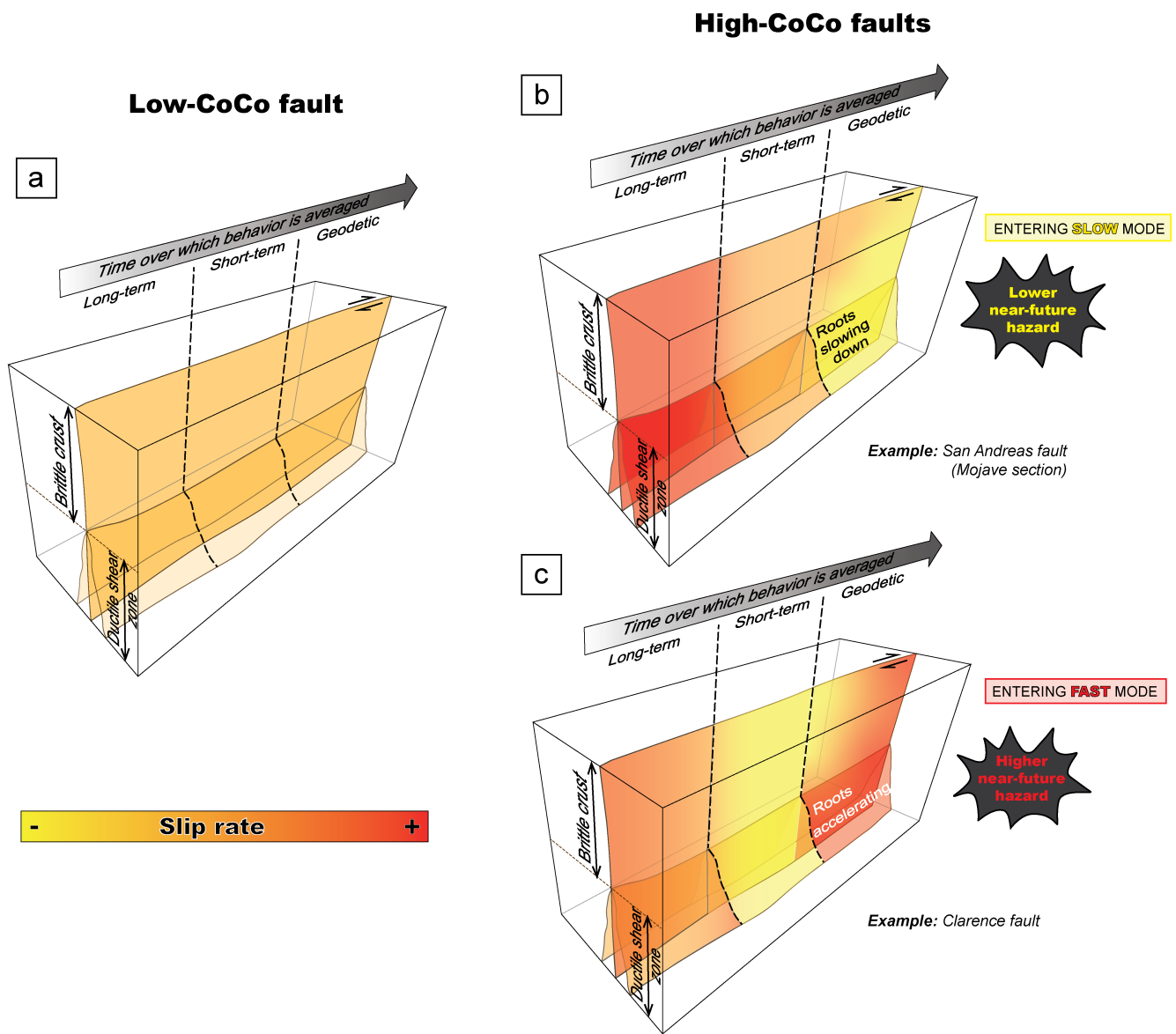
Low-CoCo fault

Figure 4 Observed modes of fault behavior, with time shown as the horizontal dimension of the block, and with relative slip rate displayed with a color gradient. In **(a)**, we show that whatever the time over which its behavior is averaged, a low-CoCo fault's slip rate is constant and thus equals its elastic strain accumulation rate, as shown in the left hand-side, hence the same color at each point in time and in the brittle and ductile parts of the fault. Note that we are not considering single-earthquake time scales. In contrast, high-CoCo faults (**b** and **c**) exhibit several types of behaviors, as discussed in the text. In **(b)**, we illustrate a fault that has a short-term (small-displacement) geologic slip rate that is slower than its long-term (large-displacement) rate. For this fault, the current elastic strain accumulation (ductile shear of the ductile roots) is slower than the short-term geologic slip rate, and therefore might be entering what we refer to as a slow mode. In **(c)**, we show another example of a fault whose long-term geologic slip rate is faster than its short-term geologic slip rate. This fault is entering a fast mode since its elastic strain accumulation is much faster than its short-term geologic slip rate.

the past 5,400 years through to the present may be masking a switch of the Wairau fault from a fast mode between 2 and 5 ka, to the current slow mode that has prevailed since the MRE at 2 ka. In both the Wairau and Garlock faults examples, if we were to use the inferred most recent geologic slip rate of 0 mm/yr as the best representation of the small-displacement slip rate, the geodetic/small-displacement rate ratios would soar, as the dashed arrows in Figure 3a illustrate.

Another example is the Yammouneh fault (14), which has a geodetic slip-deficit rate (2.5±0.5 mm/yr; Gomez et al., 2020) that is much slower than its small-

displacement slip rate (5.5±2.0 mm/yr; Daëron et al., 2004) (Figure 3). The Yammouneh fault might therefore also be experiencing a slow mode since the MRE in 1202 C.E. (Daëron et al., 2007, Table S1).

Although the small-displacement slip-rate of the Hope fault ($8.2^{+5.4}_{-3.0}$ mm/yr; Hatem et al., 2020) is likely faster than the geodetic slip-deficit rate estimate ($5.8^{+1.8}_{-1.1}$ mm/yr; Johnson et al., 2022), their respective 2σ uncertainties overlap (Table 1), which does not allow us to strongly affirm a potential switch of mode for this fault. However, the difference between these estimates might suggest that the Hope fault is currently in a slower
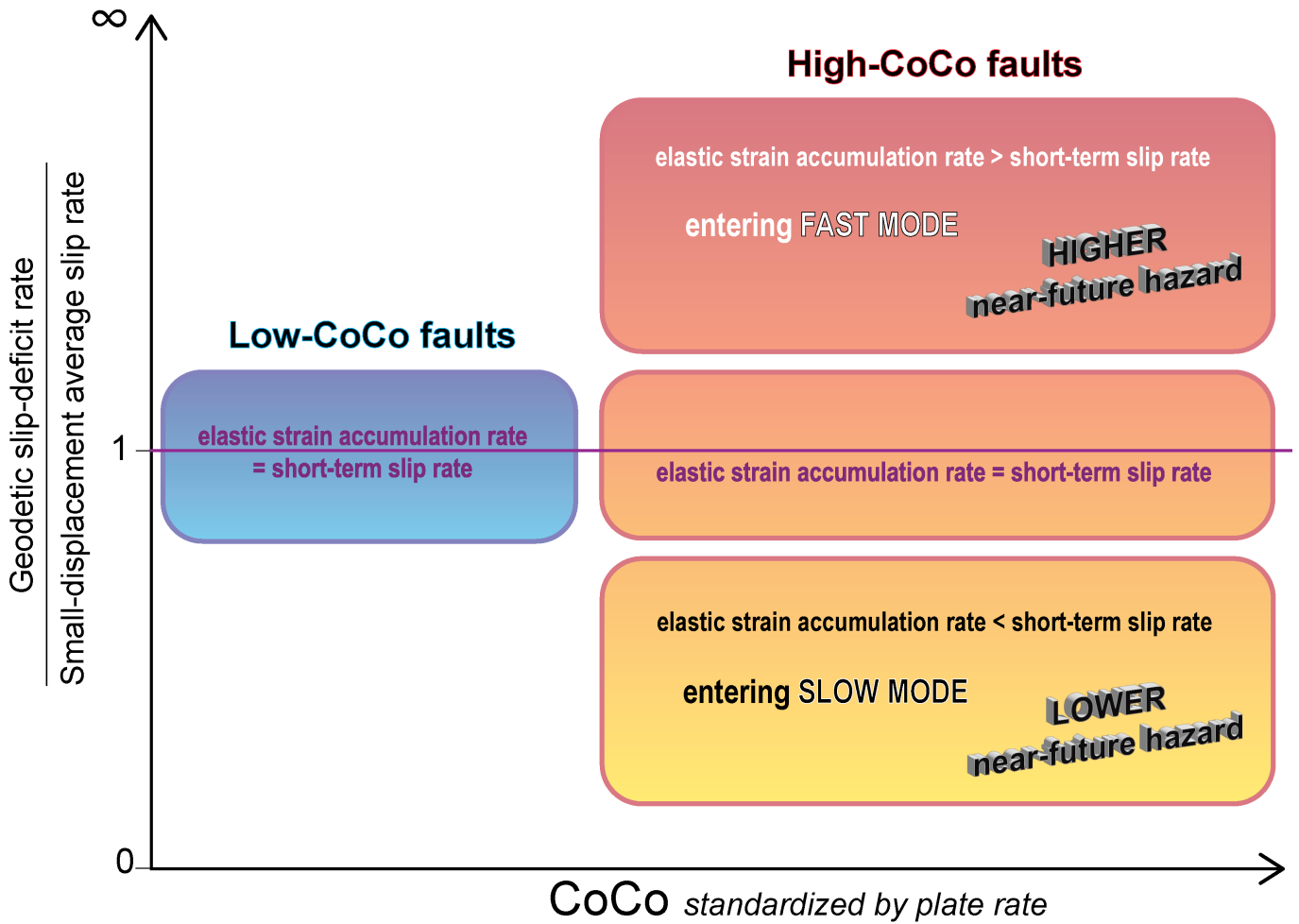
Figure 5 Schematic illustration of modes of behavior defined in this paper, according to the CoCo values and the geodetic/geologic rate ratio, and their potential meaning in terms of near-future hazard.

mode, and may have exhausted its strain capacitor in the past five earthquakes, which generated 20-30 m of fault slip over the past ~1,500 years (Hatem et al., 2019, 2020). The thus-reduced shear stress stored in the crust surrounding the Hope fault might explain the lack of significant slip on the Hope fault in the 2016 Kaikōura earthquake sequence (e.g., Hamling et al., 2017), despite its proximity to the faults that initially ruptured in the sequence. Indeed, both Ulrich et al. (2019) and Nicol et al. (2023) have suggested that the lack of significant 2016 coseismic slip on the Hope fault could be due to the low stresses in play across the Hope fault prior to the Kaikōura earthquake.

A final example is the Mojave section of the San Andreas fault (SAFm), which is characterized by an elastic strain accumulation rate (15.1±2.3 mm/yr; Evans, 2017b) that is much slower than its small-displacement slip rate (~27-29 mm/yr; Weldon et al., 2004; Dolan et al., 2016) (Figures 3, 4, Table 1). The MRE occurred 167 years ago on the SAFm, whereas the mean recurrence interval for this stretch of the fault is about 100 years (e.g., Scharer et al., 2017). The absence of any earthquakes since the 1857 MRE led to much speculation in earlier decades, when some scientists suggested that the SAFm was "overdue" (e.g., Weldon and Sieh, 1985).

These early ideas of earthquake recurrence patterns were based on the assumption of steady elastic strain accumulation rates. If, instead, elastic strain accumulation rates vary, as we show here, then the long elapsed time since the 1857 earthquake may at least partially be a consequence of reduced loading rates in this section of the SAF, as reflected in the current geodetic rate. All of this suggests that the SAFm (2) may have entered a "quieter mode".

A partial, potential alternative explanation for this situation was provided in Hearn et al. (2013) and Hearn (2022), who suggested that some of this slow elastic strain deformation rate on the SAFm might be due to a so-called "ghost transient" related to long-term viscoelastic relaxation of the lithospheric mantle and lower crust following the 1857 Fort Tejon earthquake. However, this would only explain 5 mm/yr of the apparent ~14 mm/yr difference between the geodetic slip-deficit rate and the small-displacement slip rate. In marked contrast to the SAFm, Hearn et al. (2013) also noted that there is no such "ghost transient" associated with the Garlock fault, which ruptured most recently in 1450-1640 CE (Dawson et al., 2003).

Our analysis reveals another type of behavior, in which faults exhibit geodetic slip-deficit rates that are

faster than their geologic slip rates. We suggest that these faults may have switched from a slow mode to a fast mode. This behavior characterizes the Clarence fault (9), the northern Dead Sea fault (nDSF - 13), the northern strand of the North Anatolian fault system (nNAF - 23), and the Pazarcık segment of the East Anatolian fault (EAF – 24) (Figure 3). The Clarence fault (9) has a geodetic slip-deficit rate ($8.6^{+1.5}_{-1.1}$ mm/yr; Johnson et al., 2022) that is faster than both its small-displacement and large-displacement geologic rates, although its small-displacement slip rate (2.0 ± 0.4 mm/yr) is half as fast as its large-displacement slip rate (4.2 ± 0.5 mm/yr; Zinke et al., 2019). Similarly, the nDSF stores elastic strain energy at a rate of 4.8 ± 0.3 mm/yr (Gomez et al., 2020) and is characterized by a slower small-displacement slip rate of 3.5 ± 0.2 mm/yr (Wechsler et al., 2018). For the nNAF, considering the large uncertainties on the large-displacement geologic slip rate ($18.5^{+10.9}_{-5.9}$ mm/yr, measured over a 500 My time scale; Kurt et al., 2013), we cannot confidently infer that it is slower than the reported geodetic slip-deficit rate (28.6 mm/yr; DeVries et al., 2016), but we can more confidently state that the small-displacement geologic rate (15 ± 6 mm/yr; Meghraoui et al., 2012) is slower that the geodetic rate, as suggested by Dolan and Meade (2017). The EAF (24) has a geodetic slip-deficit rate (10.3 ± 0.6 mm/yr; Aktug et al., 2016) that is nearly twice as fast as the available large-displacement geologic slip rate (5.6 ± 0.3 mm/yr; Yönlü and Karabacak, 2023). Notably, this section of the EAF ruptured in the 2023 M_w 7.8 Kahramanmaraş earthquake.

The Calico fault (6) may also fall within this type of behavior, with a switch from a previous slow mode to a current faster mode. Although the data currently available for the Calico fault do not allow us to infer a small-displacement slip rate, the current loading rate (7.4±3.4 mm/yr; Evans, 2017b) is much faster than its large-displacement slip rate (1.6±0.2 mm/yr; Oskin et al., 2007) (Figure 3). Specifically, the Calico fault has generated four surface-rupturing earthquakes within the past ~9,000 years (Ganev et al., 2010), which coincide with periods of clustered moment release identified on other faults in the eastern California shear zone (ECSZ) (Rockwell et al., 2000). The MRE on the Calico fault occurred sometime between 0.6 and 2 ka, likely as part of an ongoing cluster of earthquakes that has been occurring over the past 1-1.5 ky in the ECSZ (Rockwell et al., 2000), including most recently the 1872 Owens Valley, 1992 Landers, 1999 Hector Mine, and 2019 Ridgecrest earthquakes. Geodetic data suggest that the Calico fault, and potentially other nearby faults in the ECSZ, are likely experiencing a period of anomalously fast loading (Oskin et al., 2007; Dolan et al., 2007), as originally suggested by Peltzer et al. (2001), and further discussed by Oskin et al. (2008). Peltzer et al. (2001) showed that active dextral shear associated with the ECSZ extends across the Garlock fault, which does not exhibit any accumulation of left-lateral shear strain energy, emphasizing the idea that the Garlock fault has entered a slow mode (Evans et al., 2016; Evans, 2017a). These observations are consistent with kinematic models that suggest that the Garlock fault is currently storing and releasing

elastic strain energy at much slower-than-average rates, whereas the ECSZ subsystem is storing and releasing energy at faster-than-average rates (Dolan et al., 2007, 2016; Hatem and Dolan, 2018; Peltzer et al., 2001). Farther north in the ECSZ-Walker Lane system, the Owens Valley fault exhibits a geodetic slip-deficit rate estimate (2.7±1.4 mm/yr; Evans, 2017b) that may be faster than its small-displacement slip-rate (1.3±0.8 mm/yr; Haddon et al., 2016), consistent with a period of faster-than-average elastic strain accumulation. It is worth noting however, that these rate estimates overlap at 95% uncertainty (Table 1).

In addition to these behaviors, the San Jacinto fault (4) exhibits a small-displacement geologic slip rate (15.6±2.3 mm/yr; Onderdonk et al., 2015) that is similar to the current loading rate (13.2±4.6 mm/yr; Evans, 2017b) within 2σ uncertainties. However, there is currently no well-constrained, large-displacement (> 50 m) geologic slip rate available for the San Jacinto fault. Thus, the similarity of the geodetic and small-displacement geologic rates might suggest that the San Jacinto fault may have been captured in the middle of either a fast period (i.e., cluster) or a slow period, but in the absence of a large-displacement slip rate, we cannot say definitively which.

It is worth noting that the slip rate of high-CoCo faults does not seem to affect their behavior; both fast-slipping and slow-slipping high-CoCo faults exhibit significant dispersion of geodetic/geologic ratios. Dispersion analysis indicates that fast-slipping, high-CoCo faults exhibit larger dispersion of geodetic/geologic ratios than for slower-slipping high-CoCo faults (see Supplementary Materials), contrary to what Cowie et al. (2012) obtained from their simulations of elastic interactions between growing faults. However, we suspect that the dispersion values we determine are not particularly meaningful given the dearth of slip-rate data from fast-slipping, high-CoCo faults.

One key element to highlight is the potential difficulty in capturing any switches from fast to slow mode (or vice versa) with the available incremental fault slip-rate data, which in some instances may not be detailed enough over the appropriate displacement intervals to capture these switches in mode. This challenge will typically lie in the resolution at which the increments of the incremental slip-rate record are obtained, and if the slip-rate data are not detailed enough over the appropriate time and displacement intervals, the switches in mode may not be observable. Assuming, however, that the input data we use in this study provide sufficient information to constrain the timing of these switches in mode, our results imply that the elastic strain accumulation rate keeps up with or controls fast and slow fault slip periods, which challenges the suggestion by Weldon et al. (2004) that the strain release rate varies while the strain accumulation rate does not (i.e., their "strain-predictable behavior").

7 Ductile shear zone behavior...

7.1 ...on high-CoCo faults

The variations in strain accumulation rate described above likely record variations in the rate of shear along the ductile shear zone roots of seismogenic faults. Here we discuss the mechanisms that might control the behavior of ductile shear zones on high-CoCo faults.

The different behaviors exhibited by the high-CoCo faults can be explained by mechanisms that occur at the plate-boundary scale, such as the shared accommodation of slip in complex plate-boundary structural settings (Peltzer et al., 2001; Dolan et al., 2016), as well as by mechanisms at the scale of the fault zone, with potential strengthening and weakening processes over the ductile shear zone and the coupling between the brittle and the ductile parts of a fault (e.g., Peltzer et al., 2001; Oskin et al., 2008; Dolan et al., 2007). In structurally complex, high-CoCo settings, mechanically complementary faults within the system can share the load by trading off slip while maintaining a relatively constant overall system-level rate that keeps pace with the relative plate-motion rate (Dolan et al., 2024). In these structurally complex plate-boundary fault systems, when one fault slips much faster than its average rate throughout multiple earthquakes, the other faults of the system slip more slowly or not at all as the overall fault system works together to maintain constant average rate. Acceleration of the ductile shear zone rate will create a positive feedback loop in which faster shear on the ductile shear zone roots will drive the occurrence of more frequent, large earthquakes (i.e., an earthquake cluster) in the seismogenic part of the fault, which will in turn accelerate underlying ductile shear rates through viscous coupling, increasing driving stress, and potentially by addition of fluids into the nominally ductile uppermost parts of the ductile shear zone roots (Ellis and Stöckhert, 2004; Cowie et al., 2012; Mildon et al., 2022; Dolan et al., 2007). But eventually, either through exhaustion of the crustal strain capacitor of stored elastic strain energy on the fault in question, and/or through increases in ductile shear zone strength (i.e., resistance to shear), the fault will enter a slow mode of strain release as deformation shifts to a mechanically complementary, weaker fault within the system (Dolan et al., 2024).

These accelerations and/or decelerations of the faults' ductile shear roots of a complex fault network might be explained by strength changes (e.g., strain hardening and weakening). Dolan et al. (2007, 2016) and Dolan and Meade (2017), for instance, suggested that ductile shear zone roots can harden during fast slip periods, leading to lulls in ductile shear and hence earthquake lulls in the upper crust. In this model, the ductile shear roots of faults are accumulating elastic strain energy more slowly than their long-term slip rate, after having been "exhausted" during a period of rapid ductile shearing and fast fault slip in clusters of earthquakes (Dolan et al., 2024). Other potential mechanisms occurring within ductile shear zones that could give rise to a change in shearing rate and associated elastic strain accumulation rates of the overlying fault include changes

in fluid concentration (e.g., Mancktelow and Pennacchioni, 2004; Okazaki et al., 2021), changes in grain size (e.g., Handy, 1989; Okudaira et al., 2017), macroscopic fault evolution (e.g., Handy et al., 2007) and fabric development (e.g., Carreras et al., 2005; Melosh et al., 2018) (see Cawood and Dolan, submitted, for details on these mechanisms). All these mechanisms could drive the crustal "strain capacitor" to either its exhaustion or its replenishment (Dolan et al., 2024; Cawood and Dolan, submitted).

7.2 ...on low-CoCo faults

In contrast, tectonically isolated, primary low-CoCo plate-boundary faults (e.g. central SAF, central and eastern NAF, Alpine fault), are characterized by interseismic rates that correlate well with geologic slip rates that are averaged over both small and large displacements (Figure 3). This suggests that such low-CoCo faults must "keep up" with the relative plate-motion rate over short time and small displacement scales because there are no other mechanically complementary faults in such systems to share the load. In other words, even though all of the potential strengthening and weakening mechanisms we discuss for high-CoCo faults must be operating on low-CoCo faults as well, these processes will be overwhelmed by steady increases in driving stress related to relative plate motion. All or most of the relative plate motion must be accommodated on the primary fault in the absence of other major faults that could potentially share the work required to move the plates past each other. Moreover, the similarity of geodetic slip-deficit rates and small-displacement geologic slip rates on low-CoCo faults requires that the fault responds to steady increases in driving stress at scales of no more than a few tens of meters of relative plate motion. This is consistent with the long-held notion embodied in elastic rebound theory (Reid, 1910) that the crust can only store a given amount of elastic strain energy before the weakest element of the system (i.e., the structurally isolated primary fault) slips in an earthquake. In turn, this line of reasoning implies that the single, isolated fault either has to be weak all the time - as soon as it stores no more than a few tens of meters of elastic strain energy, it is ready to slip - or it cyclically becomes weak when stress is approaching the rupture limit. A key question is whether this near-1:1 relationship between "energy in" (as manifest in geodetic slip-deficit rates) and "energy out" (i.e., fault slip rates) on low-CoCo faults extends to single-earthquake scales. The few available earthquake-by-earthquake age plus displacement-per-event datasets that are available from low-CoCo faults suggest that, at least generally, this may be the case. Specifically, the relatively regular timing (CoV ~ 0.3) of surface ruptures on the Alpine fault at Hokuri Creek, coupled with similar ~7.5 m horizontal displacements in the two most recent earthquakes (Berryman et al., 2012; De Pascale and Langridge, 2012; Sutherland et al., 2006), and the similar displacements in the four most recent earthquakes and relatively regular timing of earthquakes on the NAF at Demir Tepe (Kondo et al., 2010) are consistent with the idea that this may extend to sin-

gle earthquake scales. If this is generally true, then low-CoCo faults may release much of, and perhaps almost all, of the shear stress accumulated since the previous event during each rupture. It is worth noting, however, that even at the Hokuri Creek site on the low-CoCo Alpine fault (Berryman et al., 2012), which is characterized by quasi-periodic earthquake recurrence, the 24-event record cannot be fit precisely with either time- or slip-predictable models (Shimazaki and Nakata, 1980), and may best be explained by an underlying chaotic behavior (Gauriau et al., 2023).

8 Fault's near-future behavior, and further applications for PSHA

Our results may provide new insight into how slip rates can be better used as basic inputs into probabilistic seismic hazard assessment (PSHA) methods. For low-CoCo faults, the outcome is straightforward – both the slip rate averaged over large displacements and the slip rate averaged over small displacements are similar to the geodetic slip-deficit rate. Therefore, any of these values can be used as an input into a PSHA. Despite this relative constancy of both strain accumulation and release rates in the behavior of a low-CoCo fault, any attempt towards formulating earthquake prediction focused on timing of earthquake occurrence on a specific fault may be functionally impossible (e.g., Chen et al., 2020; Gauriau et al., 2023). Therefore, a probabilistic methodology is required for any seismic hazard assessment.

For high-CoCo faults, the outcome is less straightforward, since such faults exhibit variable strain accumulation and release rates through time. The question arises as to what slip-rate value is the best to use in PSHA? There are three possible strategies for incorporating incremental slip-rate data into PSHA, as originally suggested by van Dissen (2020): (a) incorporating the large-displacement average slip rate by neglecting any incremental rate changes, which in a long-term statistical sense can be viewed as variations about the mean rate; (b) using the full error range associated with all available incremental slip rates, or (c) favoring the most recent (smallest-displacement multiple-earthquake) incremental slip rate as the most appropriate one.

Here we propose a potential solution to this conundrum by comparing the small-displacement and large-displacement rates with the elastic strain accumulation rates. Geodetic slip-deficit rates have been suggested as primary inputs into seismic hazard assessment (e.g., Bird and Kreemer, 2014; Hussain et al., 2018), but never in light of comparison to available geologic slip-rate records. The examples listed in paragraph 6.2., however, illustrate the current limitations on using small-displacement rates (suggestion c) as a proxy for the most recent phase of fault behavior without considering the possibility that the fault may have switched modes in the interval since displacement of the most-recent available small-displacement slip-rate data. We suggest that a potential path forward is to use the comparison of the geodetic slip-deficit rates with small-

displacement geologic rates of high-CoCo faults to forecast the near-future behavior that might be expected on a given fault. While we suggested in our earlier paper (Gauriau and Dolan, 2021) that option (c), i.e., implementing the shorter-term slip rate into a PSHA, would lead to a more reliable forecast of the near-future behavior of the fault, the current analysis suggests that deviations of geodetic rates from the small-displacement geologic slip rates might better illustrate the future behavior of high-CoCo faults.

Specifically, we propose that a geodetic slip-deficit rate that is slower than the small-displacement slip rate might indicate lower near-future hazard, because the fault is storing elastic strain energy more slowly than average (Figure 5). This is exemplified by the cases of the Garlock fault, the SAFm, and the Hope fault. Conversely, geodetic rates that are faster than the small-displacement rate on faults that have not experienced a recent earthquake (i.e., those not experiencing a post-seismic strain transient) may indicate higher near-future hazard, as illustrated by the nNAF, the Clarence fault, and the nDSF. In support of this idea, the 2023 M_w 7.8 Kahramanmaraş earthquake occurred on a section of the EAF that exhibited a geodetic slip-deficit rate, prior to the earthquake, that was almost twice as fast as the long-term geologic slip rate. In the case of the San Jacinto fault, and other faults with a geodetic rate that equals the small-displacement slip rate, we suggest that the near-future hazard can be best represented by the small-displacement slip rate and/or the geodetic rate (Figure 5).

One possible route towards using these observations in improved PSHA would be to evaluate geodetic and geologic rate discrepancies using the smallest-displacement incremental slip rate for a fault to infer the current mode of fault behavior.

9 Conclusions

Our comparison of geologic fault slip rates with geodetic slip-deficit rates from strike-slip plate-boundary faults reveals markedly different strain accumulation and release behavior on structurally isolated faults relative to those that extend through structurally complex regions. Our main take-away is that elastic strain accumulation rates on high-CoCo faults must vary through time, whereas they remain relatively constant on low-CoCo faults. This can potentially be applied to faults exhibiting other kinematics, such as extensional or compressional fault systems, where both fault interactions and slip-rate variability have also been studied (e.g., Luo and Liu, 2010; Mildon et al., 2022).

High-CoCo faults have geodetic-to-geologic ratios that vary widely, demonstrating that rates of elastic strain accumulation vary significantly through time at scales that are longer than individual earthquake cycles. This is particularly clear from the differences observed between the short-term geodetic slip-deficit rate data with long-term, large-displacement geologic slip rates, which will average over any shorter-term and smaller-displacement accelerations and decelerations of fault slip that typify faults in such settings (Gauriau

and Dolan, 2021). Presumably, these changes reflect temporally variable rates of shear on the ductile shear zone roots of brittle faults, which we infer are related to the more complicated history of strain accumulation and release among regional fault interactions at displacement scales of a few tens of meters and centennial to millennial time scales. Specifically, geodetic slip-deficit rates that neither match large-displacement nor small-displacement average slip rates indicate that the elastic strain accumulation rate must vary over time scales corresponding to the deceleration and acceleration periods over which smallest-displacement geologic rates are averaged.

In contrast, low-CoCo faults are characterized by steady elastic strain accumulation and release rates, which indicate that such faults need to "keep up with" the relative plate motion rate at short-time and small-displacement scales, overwhelming any potential strengthening and weakening mechanisms that might be operating on such faults. Consequently, the geodetic slip-deficit rate observed on a low-CoCo fault can be used as a proxy for its geologic rate, which itself can be assumed to be relatively constant.

Finally, we suggest that the discrepancies between short-term geologic slip rates and geodetic slip-deficit rates for high-CoCo faults might represent a switch of mode, revealing either an accelerating or a decelerating phase. A geodetic slip-deficit rate that is faster than the most recent geologic incremental slip rate would imply a potential higher near-future seismic hazard, whereas a geodetic rate that is slower than the smallest-displacement slip rate would signal a lower near-future seismic hazard. These discrepancies could be used to refine PSHA models, not only in strike-slip fault systems, as highlighted in this study, but potentially to any type of plate-boundary kinematics. The importance and current relative dearth of robust incremental slip rate records highlights the need to develop more such records from more faults around the world to enable better PSHA.

Acknowledgements

10 Data and code availability

The data used in this study, and necessary to reproduce our results, are all part of published articles, referred to in Table 1 and throughout the manuscript.

11 Competing interests

The authors have no competing interests.

References

Aktug, B., Ozener, H., Dogru, A., Sabuncu, A., Turgut, B., Halicioglu, K., Yilmaz, O., and Havazli, E. Slip rates and seismic potential on the East Anatolian Fault System using an improved GPS velocity field. *Journal of Geodynamics*, 94–95:1–12, Mar. 2016. doi: 10.1016/j.jog.2016.01.001.

Barbot, S., Luo, H., Wang, T., Hamiel, Y., Piatibratova, O., Javed, M. T., Braitenberg, C., and Gurbuz, G. Slip distribution of the February 6, 2023 Mw 7.8 and Mw 7.6, Kahramanmaraş, Turkey earthquake sequence in the East Anatolian Fault Zone. *Seismica*, 2(3), Apr. 2023. doi: 10.26443/seismica.v2i3.502.

Barka, A. The North Anatolian fault zone. *Annales tectonicae*, suppl. VI:164–195, 1992.

Barka, A., Akyüz, H., Altunel, E., Sunal, G., Cakir, Z., Dikbas, Aand Yerli, B., Armijo, R., Meyer, B., de Chabalier, J., Rockwell, T., Dolan, J., Hartleb, R., Dawson, T., Christofferson, S., Tucker, A., Fumal, T., Langridge, R., Stenner, H., Lettis, W., Bachhuber, J., and Page, W. The Surface Rupture and Slip Distribution of the 17 August 1999 Izmit Earthquake (M 7.4), North Anatolian Fault. *Bulletin of the Seismological Society of America*, 92(1): 43–60, Feb. 2002. doi: 10.1785/0120000841.

Barth, N., Kulhanek, D., Beu, A., Murray-Wallace, C., Hayward, B., Mildenhall, D., and Lee, D. New c. 270 kyr strike-slip and uplift rates for the southern Alpine Fault and implications for the New Zealand plate boundary. *Journal of Structural Geology*, 64: 39–52, 2014. doi: 10.1016/j.jsg.2013.08.009.

Bender, A. M., Lease, R. O., Rittenour, T., and Jones, J. V. Rapid active thrust faulting at the northern Alaska Range front. *Geology*, 51(6):527–531, Mar. 2023. doi: 10.1130/G51049.1.

Bendick, R., Bilham, R., Freymueller, J., Larson, K., and Yin, G. Geodetic evidence for a low slip rate in the Altyn Tagh fault system. *Nature*, 404(6773):69–72, Mar. 2000. doi: 10.1038/35003555.

Benedetti, L., Finkel, R., Papanastassiou, D., King, G., Armijo, R., Ryerson, F., Farber, D., and Flerit, F. Post-glacial slip history of the Sparta fault (Greece) determined by 36 Cl cosmogenic dating: Evidence for non-periodic earthquakes. *Geophysical Research Letters*, 29(8), Apr. 2002. doi: 10.1029/2001gl014510.

Berryman, K. R., Cochran, U. A., Clark, K. J., Biasi, G. P., Langridge, R. M., and Villamor, P. Major Earthquakes Occur Regularly on an Isolated Plate Boundary Fault. *Science*, 336(6089):1690–1693, June 2012. doi: 10.1126/science.1218959.

Bird, P. and Kreemer, C. Revised Tectonic Forecast of Global Shallow Seismicity Based on Version 2.1 of the Global Strain Rate Map. *Bulletin of the Seismological Society of America*, 105(1): 152–166, Dec. 2014. doi: 10.1785/0120140129.

Brothers, D. S., Miller, N. C., Barrie, J. V., Haeussler, P. J., Greene, H. G., Andrews, B. D., Zielke, O., Watt, J., and Dartnell, P. Plate boundary localization, slip-rates and rupture segmentation of the Queen Charlotte Fault based on submarine tectonic geomorphology. *Earth and Planetary Science Letters*, 530:115882, Jan. 2020. doi: 10.1016/j.epsl.2019.115882.

Bull, J., Barnes, P., Lamarche, G., Sanderson, D., Cowie, P., Taylor, S., and Dix, J. High-resolution record of displacement accumulation on an active normal fault: implications for models of slip accumulation during repeated earthquakes. *Journal of Structural Geology*, 28(7):1146–1166, July 2006. doi: 10.1016/j.jsg.2006.03.006.

Carreras, J., Druguet, E., and Griera, A. Shear zone-related folds. *Journal of Structural Geology*, 27(7):1229–1251, July 2005. doi: 10.1016/j.jsg.2004.08.004.

Cawood, T. and Dolan, J. Fault strength variations over multiple seismic cycles: The role of fluids, cementation, strain hardening, and shear folding, submitted.

Chen, Y., Liu, M., and Luo, G. Complex Temporal Patterns of Large Earthquakes: Devil's Staircases. *Bulletin of the Seismological Society of America*, 110(3):1064–1076, Apr. 2020. doi:

10.1785/0120190148.

Cowgill, E. Impact of riser reconstructions on estimation of secular variation in rates of strike–slip faulting: Revisiting the Cherchen River site along the Altyn Tagh Fault, NW China. *Earth and Planetary Science Letters*, 254(3):239–255, Feb. 2007. doi: 10.1016/j.epsl.2006.09.015.

Cowgill, E., Gold, R. D., Xuanhua, C., Xiao-Feng, W., Arrowsmith, J. R., and Southon, J. Low Quaternary slip rate reconciles geodetic and geologic rates along the Altyn Tagh fault, northwestern Tibet. *Geology*, 37(7):647–650, July 2009. doi: 10.1130/G25623A.1.

Cowie, P. A., Roberts, G. P., Bull, J. M., and Visini, F. Relationships between fault geometry, slip rate variability and earthquake recurrence in extensional settings: Fault geometry control on earthquake rupture. *Geophysical Journal International*, 189(1): 143–160, Feb. 2012. doi: 10.1111/j.1365-246x.2012.05378.x.

Daëron, M., Benedetti, L., Tapponnier, P., Sursock, A., and Finkel, R. C. Constraints on the post ~25-ka slip rate of the Yammoûneh fault (Lebanon) using in situ cosmogenic 36Cl dating of offset limestone-clast fans. *Earth and Planetary Science Letters*, 227 (1–2):105–119, Oct. 2004. doi: 10.1016/j.epsl.2004.07.014.

Daëron, M., Klinger, Y., Tapponnier, P., Elias, A., Jacques, E., and Sursock, A. 12,000-Year-Long Record of 10 to 13 Paleoearthquakes on the Yammouneh Fault, Levant Fault System, Lebanon. *Bulletin of the Seismological Society of America*, 97(3): 749–771, June 2007. doi: 10.1785/0120060106.

Daout, S., Jolivet, R., Lasserre, C., Doin, M.-P., Barbot, S., Tapponnier, P., Peltzer, G., Socquet, A., and Sun, J. Along-strike variations of the partitioning of convergence across the Haiyuan fault system detected by InSAR. *Geophysical Journal International*, 205(1):536–547, Apr. 2016. doi: 10.1093/gji/ggw028.

Dawson, T. E., McGill, S. F., and Rockwell, T. K. Irregular recurrence of paleoearthquakes along the central Garlock fault near El Paso Peaks, California. *Journal of Geophysical Research: Solid Earth*, 108(B7), July 2003. doi: 10.1029/2001jb001744.

De Pascale, G. P. and Langridge, R. M. New on-fault evidence for a great earthquake in A.D. 1717, central Alpine fault, New Zealand. *Geology*, 40(9):791–794, June 2012. doi: 10.1130/g33363.1.

DeMets, C. and Dixon, T. H. New kinematic models for Pacific-North America motion from 3 Ma to present, I: Evidence for steady motion and biases in the NUVEL-1A Model. *Geophysical Research Letters*, 26(13):1921–1924, July 1999. doi: 10.1029/1999gl900405.

DeVries, P. M. R., Krastev, P. G., Dolan, J. F., and Meade, B. J. Viscoelastic Block Models of the North Anatolian Fault: A Unified Earthquake Cycle Representation of Pre- and Postseismic Geodetic Observations. *Bulletin of the Seismological Society of America*, 107(1):403–417, Nov. 2016. doi: 10.1785/0120160059.

Dolan, J., Van Dissen, R., Rhodes, E., Zinke, R., Hatem, A., McGuire, C., Langridge, R., and Grenader, J. One tune, many tempos: Faults trade off slip in time and space to accommodate relative plate motions. *Earth and Planetary Science Letters*, 625:118484, Jan. 2024. doi: 10.1016/j.epsl.2023.118484.

Dolan, J. F. and Meade, B. J. A Comparison of Geodetic and Geologic Rates Prior to Large Strike-Slip Earthquakes: A Diversity of Earthquake-Cycle Behaviors? *Geochemistry, Geophysics, Geosystems*, 18(12):4426–4436, Dec. 2017. doi: 10.1002/2017gc007014.

Dolan, J. F., Bowman, D. D., and Sammis, C. G. Long-range and long-term fault interactions in Southern California. *Geology*, 35 (9):855, 2007. doi: 10.1130/g23789a.1.

Dolan, J. F., McAuliffe, L. J., Rhodes, E. J., McGill, S. F., and Zinke, R. Extreme multi-millennial slip rate variations on the Garlock fault, California: Strain super-cycles, potentially time-variable

fault strength, and implications for system-level earthquake occurrence. *Earth and Planetary Science Letters*, 446:123–136, July 2016. doi: 10.1016/j.epsl.2016.04.011.

Elliott, J. and Freymueller, J. T. A Block Model of Present-Day Kinematics of Alaska and Western Canada. *Journal of Geophysical Research: Solid Earth*, 125(7):e2019JB018378, 2020. doi: 10.1029/2019JB018378.

Ellis, S. and Stöckhert, B. Elevated stresses and creep rates beneath the brittle-ductile transition caused by seismic faulting in the upper crust. *Journal of Geophysical Research: Solid Earth*, 109(B5), May 2004. doi: 10.1029/2003jb002744.

Evans, E. L. Persistent slip rate discrepancies in the eastern California (USA) shear zone: Reply. *Geology*, 45(9):e426–e426, Sept. 2017a. doi: 10.1130/g39439y.1.

Evans, E. L. A Comprehensive Analysis of Geodetic Slip-Rate Estimates and Uncertainties in California. *Bulletin of the Seismological Society of America*, 108(1):1–18, Nov. 2017b. doi: 10.1785/0120170159.

Evans, E. L., Thatcher, W. R., Pollitz, F. F., and Murray, J. R. Persistent slip rate discrepancies in the eastern California (USA) shear zone. *Geology*, 44(9):691–694, July 2016. doi: 10.1130/g37967.1.

Fougere, D., Dolan, J. F., Rhodes, E., McGill, S. F., and Ivester, A. Deciphering Non-Constant Earthquake Behavior: Insights from the Garlock Fault in Southern California. 2023. https://agu.confex.com/agu/fm23/meetingapp.cgi/Paper/1283318.

Fougere, D., Dolan, J. F., Rhodes, E. J., and McGill, S. F. Refined Holocene slip rate for the western and central segments of the Garlock fault: Record of Alternating Millenial-Scale Periods of Fast and Slow Fault Slip, submitted.

Friedrich, A. M., Wernicke, B. P., Niemi, N. A., Bennett, R. A., and Davis, J. L. Comparison of geodetic and geologic data from the Wasatch region, Utah, and implications for the spectral character of Earth deformation at periods of 10 to 10 million years. *Journal of Geophysical Research: Solid Earth*, 108(B4), Apr. 2003. doi: 10.1029/2001jb000682.

Ganev, P. N., Dolan, J. F., Blisniuk, K., Oskin, M., and Owen, L. A. Paleoseismologic evidence for multiple Holocene earthquakes on the Calico fault: Implications for earthquake clustering in the Eastern California shear zone. *Lithosphere*, 2(4):287–298, Aug. 2010. doi: 10.1130/l82.1.

Gauriau, J. and Dolan, J. F. Relative Structural Complexity of Plate-Boundary Fault Systems Controls Incremental Slip-Rate Behavior of Major Strike-Slip Faults. *Geochemistry, Geophysics, Geosystems*, 22(11), Nov. 2021. doi: 10.1029/2021gc009938.

Gauriau, J., Barbot, S., and Dolan, J. F. Islands of chaos in a sea of periodic earthquakes. *Earth and Planetary Science Letters*, 618: 118274, Sept. 2023. doi: 10.1016/j.epsl.2023.118274.

Gomez, F., Meghraoui, M., Darkal, A., Hijazi, F., Mouty, M., Suleiman, Y., Sbeinati, R., Darawcheh, R., Al-Ghazzi, R., and Barazangi, M. Holocene faulting and earthquake recurrence along the Serghaya branch of the Dead Sea fault system in Syria and Lebanon. *Geophys J Int*, 153(3):658–674, June 2003. doi: 10.1046/j.1365-246X.2003.01933.x.

Gomez, F., Nemer, T., Tabet, C., Khawlie, M., Meghraoui, M., and Barazangi, M. Strain partitioning of active transpression within the Lebanese restraining bend of the Dead Sea Fault (Lebanon and SW Syria). *Geological Society, London, Special Publications*, 290(1):285–303, Jan. 2007. doi: 10.1144/290.10.

Gomez, F., Cochran, W. J., Yassminh, R., Jaafar, R., Reilinger, R., Floyd, M., King, R. W., and Barazangi, M. Fragmentation of the Sinai Plate indicated by spatial variation in present-day slip rate along the Dead Sea Fault System. *Geophysical Journal International*, 221(3):1913–1940, Feb. 2020. doi: 10.1093/gji/ggaa095.

Grant Ludwig, L., Akciz, S. O., Arrowsmith, J. R., and Salisbury, J. B. Reproducibility of San Andreas Fault Slip Rate Measurements at Wallace Creek in the Carrizo Plain, CA. *Earth and Space Science*, 6(1):156–165, Jan. 2019. doi: 10.1029/2017ea000360.

Güvercin, S. E., Karabulut, H., Konca, A. O., Doğan, U., and Ergintav, S. Active seismotectonics of the East Anatolian Fault. *Geophysical Journal International*, 230(1):50–69, July 2022. doi: 10.1093/gji/ggac045.

Haddon, E. K., Amos, C. B., Zielke, O., Jayko, A. S., and Bürgmann, R. Surface slip during large Owens Valley earthquakes. *Geochemistry, Geophysics, Geosystems*, 17(6):2239–2269, June 2016. doi: 10.1002/2015gc006033.

Haeussler, P. J. Surface Rupture and Slip Distribution of the Denali and Totschunda Faults in the 3 November 2002 M 7.9 Earthquake, Alaska. *Bulletin of the Seismological Society of America*, 94(6B):S23–S52, Dec. 2004. doi: 10.1785/0120040626.

Haibing, L., Van der Woerd, J., Tapponnier, P., Klinger, Y., Xuexiang, Q., Jingsui, Y., and Yintang, Z. Slip rate on the Kunlun fault at Hongshui Gou, and recurrence time of great events comparable to the 14/11/2001, Mw⊠7.9 Kokoxili earthquake. *Earth and Planetary Science Letters*, 237(1):285–299, Aug. 2005. doi: 10.1016/j.epsl.2005.05.041.

Hamiel, Y., Piatibratova, O., Mizrahi, Y., Nahmias, Y., and Sagy, A. Crustal Deformation across the Jericho Valley Section of the Dead Sea Fault as Resolved by Detailed Field and Geodetic Observations. *Geophysical Research Letters*, 45(7):3043–3050, 2018. doi: 10.1002/2018GL077547.

Hamling, I. J., Hreinsdóttir, S., Clark, K., Elliott, J., Liang, C., Fielding, E., Litchfield, N., Villamor, P., Wallace, L., Wright, T. J., D'Anastasio, E., Bannister, S., Burbidge, D., Denys, P., Gentle, P., Howarth, J., Mueller, C., Palmer, N., Pearson, C., Power, W., Barnes, P., Barrell, D. J. A., Van Dissen, R., Langridge, R., Little, T., Nicol, A., Pettinga, J., Rowland, J., and Stirling, M. Complex multifault rupture during the 2016 M w 7.8 Kaikōura earthquake, New Zealand. *Science*, 356(6334), Apr. 2017. doi: 10.1126/science.aam7194.

Handy, M. R. Deformation regimes and the rheological evolution of fault zones in the lithosphere: the effects of pressure, temperature, grainsize and time. *Tectonophysics*, 163(1–2):119–152, June 1989. doi: 10.1016/0040-1951(89)90122-4.

Handy, M. R., Hirth, G., and Bürgmann, R. Continental Fault Structure and Rheology from the Frictional-to-Viscous Transition Downward. In *Tectonic Faults*, page 139–182. The MIT Press, May 2007. doi: 10.7551/mitpress/6703.003.0008.

Hatem, A. E. and Dolan, J. F. A Model for the Initiation, Evolution, and Controls on Seismic Behavior of the Garlock Fault, California. *Geochemistry, Geophysics, Geosystems*, 19(7):2166–2178, July 2018. doi: 10.1029/2017gc007349.

Hatem, A. E., Dolan, J. F., Zinke, R. W., Van Dissen, R. J., McGuire, C. M., and Rhodes, E. J. A 2000 Yr Paleoearthquake Record along the Conway Segment of the Hope Fault: Implications for Patterns of Earthquake Occurrence in Northern South Island and Southern North Island, New Zealand. *Bulletin of the Seismological Society of America*, 109(6):2216–2239, Sept. 2019. doi: 10.1785/0120180313.

Hatem, A. E., Dolan, J. F., Zinke, R. W., Langridge, R. M., McGuire, C. P., Rhodes, E. J., Brown, N., and Van Dissen, R. J. Holocene to latest Pleistocene incremental slip rates from the east-central Hope fault (Conway segment) at Hossack Station, Marlborough fault system, South Island, New Zealand: Towards a dated path of earthquake slip along a plate boundary fault. *Geosphere*, 16 (6):1558–1584, Oct. 2020. doi: 10.1130/ges02263.1.

He, J., Vernant, P., Chéry, J., Wang, W., Lu, S., Ku, W., Xia, W., and Bilham, R. Nailing down the slip rate of the Altyn Tagh

fault. *Geophysical Research Letters*, 40(20):5382–5386, 2013. doi: 10.1002/2013GL057497.

Hearn, E. "Ghost Transient" Corrections to the Southern California GPS Velocity Field from San Andreas Fault Seismic Cycle Models. *Seismological Research Letters*, 93(6):2973–2989, Aug. 2022. doi: 10.1785/0220220156.

Hearn, E. H., Pollitz, F. F., Thatcher, W. R., and Onishi, C. T. How do "ghost transients" from past earthquakes affect GPS slip rate estimates on southern California faults? *Geochemistry, Geophysics, Geosystems*, 14(4):828–838, Apr. 2013. doi: 10.1002/ggge.20080.

Hubert-Ferrari, A., Armijo, R., King, G., Meyer, B., and Barka, A. Morphology, displacement, and slip rates along the North Anatolian Fault, Turkey. *Journal of geophysical research Solid Earth*, 107 (B10):ETG 9–1–ETG 9–33, 2002. doi: 10.1029/2001JB000393.

Hussain, E., Wright, T. J., Walters, R. J., Bekaert, D. P. S., Lloyd, R., and Hooper, A. Constant strain accumulation rate between major earthquakes on the North Anatolian Fault. *Nature Communications*, 9(1), Apr. 2018. doi: 10.1038/s41467-018-03739-2.

Johnson, K. M., Wallace, L. M., Maurer, J., Hamling, I. J., Williams, C. A., Rollins, C., Gerstenberger, M. C., and Van Dissen, R. J. Geodetic deformation model for the 2022 update of the New Zealand National Seismic Hazard Model. 2022. doi: 10.21420/P93X-8293.

Kirby, E., Harkins, N., Wang, E., Shi, X., Fan, C., and Burbank, D. Slip rate gradients along the eastern Kunlun fault. *Tectonics*, 26(2), 2007. doi: 10.1029/2006TC002033.

Kirby, E., Anandakrishnan, S., Phillips, F., and Marrero, S. Late Pleistocene slip rate along the Owens Valley fault, eastern California. *Geophysical Research Letters*, 35(1), 2008. doi: 10.1029/2007GL031970.

Klinger, Y., Avouac, J., Abou Karaki, N., Dorbath, L., Bourles, D., and Reyss, J. Slip rate on the Dead Sea transform fault in northern Araba valley (Jordan). *Geophysical Journal International*, 142(3): 755–768, 2000. doi: 10.1046/j.1365-246x.2000.00165.x.

Kondo, H., Özaksoy, V., and Yıldirim, C. Slip history of the 1944 Bolu-Gerede earthquake rupture along the North Anatolian fault system: Implications for recurrence behavior of multisegment earthquakes. *Journal of Geophysical Research: Solid Earth*, 115(B4), Apr. 2010. doi: 10.1029/2009jb006413.

Kozacı, O., Dolan, J., Finkel, R., and Hartleb, R. Late Holocene slip rate for the North Anatolian fault, Turkey, from cosmogenic 36Cl geochronology: Implications for the constancy of fault loading and strain release rates. *Geological Society of America Bulletin*, 35(10):867–870, 2007.

Kozacı, O., Dolan, J. F., and Finkel, R. C. A late Holocene slip rate for the central North Anatolian fault, at Tahtaköprü, Turkey, from cosmogenic 10Be geochronology: Implications for fault loading and strain release rates. *Journal of Geophysical Research: Solid Earth*, 114(B1), Jan. 2009. doi: 10.1029/2008jb005760.

Kozacı, O., Dolan, J. F., Yönlü, O., and Hartleb, R. D. Paleoseismologic evidence for the relatively regular recurrence of infrequent, large-magnitude earthquakes on the eastern North Anatolian fault at Yaylabeli, Turkey. *Lithosphere*, 3(1):37–54, Feb. 2011. doi: 10.1130/l118.1.

Kurt, H., Sorlien, C. C., Seeber, L., Steckler, M. S., Shillington, D. J., Cifci, G., Cormier, M., Dessa, J., Atgin, O., Dondurur, D., Demirbag, E., Okay, S., Imren, C., Gurcay, S., and Carton, H. Steady late quaternary slip rate on the Cinarcik section of the North Anatolian fault near Istanbul, Turkey. *Geophysical Research Letters*, 40(17):4555–4559, Sept. 2013. doi: 10.1002/grl.50882.

Li, C., Zhang, P.-z., Yin, J., and Min, W. Late Quaternary left-lateral slip rate of the Haiyuan fault, northeastern mar-

gin of the Tibetan Plateau. *Tectonics*, 28(5), 2009. doi: 10.1029/2008TC002302.

Liu, J., Ren, Z., Zhang, H., Li, C., Zhang, Z., WenJun, Z., XueMei, L. I., and CaiCai, L. I. U. Late Quaternary slip rate of the Laohushan fault within the Haiyuan fault zone and its tectonic implications. *Chinese Journal of Geophysics*, 61(4):1281–1297, Apr. 2018. doi: 10.6038/cjg2018L0364.

Liu, J., Ren, Z., Zhang, H., Li, C., Zhang, Z., Zheng, W., Li, X., and Liu, C. Slip Rates Along the Laohushan Fault and Spatial Variation in Slip Rate Along the Haiyuan Fault Zone. *Tectonics*, 41(2): e2021TC006992, 2022. doi: 10.1029/2021TC006992.

Luo, G. and Liu, M. Stress evolution and fault interactions before and after the 2008 Great Wenchuan earthquake. *Tectonophysics*, 491(1–4):127–140, Aug. 2010. doi: 10.1016/j.tecto.2009.12.019.

Mancktelow, N. S. and Pennacchioni, G. The influence of grain boundary fluids on the microstructure of quartz-feldspar mylonites. *Journal of Structural Geology*, 26(1):47–69, Jan. 2004. doi: 10.1016/s0191-8141(03)00081-6.

Masson, F., Hamiel, Y., Agnon, A., Klinger, Y., and Deprez, A. Variable behavior of the Dead Sea Fault along the southern Arava segment from GPS measurements. *Comptes Rendus Geoscience*, 347(4):161–169, July 2015. doi: 10.1016/j.crte.2014.11.001.

Matmon, A., Schwartz, D., Haeussler, P., Finkel, R., Lienkaemper, J., Stenner, H., and Dawson, T. Denali fault slip rates and Holocene–late Pleistocene kinematics of central Alaska. *Geology*, 34(8):645–648, Aug. 2006. doi: 10.1130/G22361.1.

McGill, S. and Sieh, K. Holocene slip rate of the Central Garlock Fault in southeastern Searles Valley, California. *Journal of Geophysical Research: Solid Earth*, 98(B8):14217–14231, 1993. doi: 10.1029/93JB00442.

Meade, B. J., Klinger, Y., and Hetland, E. A. Inference of Multiple Earthquake-Cycle Relaxation Timescales from Irregular Geodetic Sampling of Interseismic Deformation. *Bulletin of the Seismological Society of America*, 103(5):2824–2835, Sept. 2013. doi: 10.1785/0120130006.

Meghraoui, M., Aksoy, M. E., Akyüz, H. S., Ferry, M., Dikbaş, A., and Altunel, E. Paleoseismology of the North Anatolian Fault at Güzelköy (Ganos segment, Turkey): Size and recurrence time of earthquake ruptures west of the Sea of Marmara. *Geochemistry, Geophysics, Geosystems*, 13(4), Apr. 2012. doi: 10.1029/2011gc003960.

Melosh, B. L., Rowe, C. D., Gerbi, C., Smit, L., and Macey, P. Seismic cycle feedbacks in a mid-crustal shear zone. *Journal of Structural Geology*, 112:95–111, July 2018. doi: 10.1016/j.jsg.2018.04.004.

Mencin, D., Bendick, R., Upreti, B. N., Adhikari, D. P., Gajurel, A., Bhattarai, R. R., Shrestha, H. R., Bhattarai, T. N., Manandhar, N., Galetzka, J., Knappe, E., Pratt-Sitaula, B., Aoudia, A., and Bilham, R. Himalayan strain reservoir inferred from limited afterslip following the Gorkha earthquake. *Nature Geoscience*, 9(7): 533–537, June 2016. doi: 10.1038/ngeo2734.

Mildon, Z. K., Roberts, G. P., Faure Walker, J. P., Beck, J., Papanikolaou, I., Michetti, A. M., Toda, S., Iezzi, F., Campbell, L., McCaffrey, K. J. W., Shanks, R., Sgambato, C., Robertson, J., Meschis, M., and Vittori, E. Surface faulting earthquake clustering controlled by fault and shear-zone interactions. *Nature Communications*, 13(1), Nov. 2022. doi: 10.1038/s41467-022-34821-5.

Nicol, A. and Dissen, R. V. A 6000-year record of surface-rupturing paleoearthquakes on the Wairau Fault, New Zealand. *New Zealand Journal of Geology and Geophysics*, 61(3):341–358, July 2018. doi: 10.1080/00288306.2018.1498360.

Nicol, A., Howell, A., Litchfield, N., Wilson, T., Bannister, S., and Massey, C. Introduction to the Kaikōura earthquake special issue. *New Zealand Journal of Geology and Geophysics*, 66(2):

137–146, Apr. 2023. doi: 10.1080/00288306.2023.2197240.

Niemi, T. M., Zhang, H., Atallah, M., and Harrison, J. B. J. Late Pleistocene and Holocene slip rate of the Northern Wadi Araba fault, Dead Sea Transform, Jordan. *Journal of Seismology*, 5(3): 449–474, July 2001. doi: 10.1023/A:1011487912054.

Noriega, G., Arrowsmith, J., Grant, L., and Young, J. Stream Channel Offset and Late Holocene Slip Rate of the San Andreas Fault at the Van Matre Ranch Site, Carrizo Plain, California. *Bulletin of the Seismological Society of America*, 96(1):33–47, 2006. doi: 10.1785/0120050094.

Okazaki, K., Burdette, E., and Hirth, G. Rheology of the Fluid Oversaturated Fault Zones at the Brittle-Plastic Transition. *Journal of Geophysical Research: Solid Earth*, 126(2), Feb. 2021. doi: 10.1029/2020jb020804.

Okudaira, T., Shigematsu, N., Harigane, Y., and Yoshida, K. Grain size reduction due to fracturing and subsequent grain-size-sensitive creep in a lower crustal shear zone in the presence of a CO2-bearing fluid. *Journal of Structural Geology*, 95:171–187, Feb. 2017. doi: 10.1016/j.jsg.2016.11.001.

Onderdonk, N. W., McGill, S. F., and Rockwell, T. K. Short-term variations in slip rate and size of prehistoric earthquakes during the past 2000 years on the northern San Jacinto fault zone, a major plate-boundary structure in southern California. *Lithosphere*, 7 (3):211–234, Feb. 2015. doi: 10.1130/l393.1.

Oskin, M., Perg, L., Blumentritt, D., Mukhopadhyay, S., and Iriondo, A. Slip rate of the Calico fault: Implications for anomalous geodetic strain accumulation across the Eastern California shear zone. 2004:G11A–0776, Dec. 2004. https://ui.adsabs.harvard.edu/abs/2004AGUFM.G11A0776O.

Oskin, M., Perg, L., Blumentritt, D., Mukhopadhyay, S., and Iriondo, A. Slip rate of the Calico fault: Implications for geologic versus geodetic rate discrepancy in the Eastern California Shear Zone. *Journal of Geophysical Research: Solid Earth*, 112(B3), Mar. 2007. doi: 10.1029/2006jb004451.

Oskin, M., Perg, L., Shelef, E., Strane, M., Gurney, E., Singer, B., and Zhang, X. Elevated shear zone loading rate during an earthquake cluster in eastern California. *Geology*, 36(6):507, 2008. doi: 10.1130/g24814a.1.

Page, C. J., Denys, P. H., and Pearson, C. F. A geodetic study of the Alpine Fault through South Westland: using campaign GPS data to model slip rates on the Alpine Fault. *New Zealand Journal of Geology and Geophysics*, 61(3):359–366, July 2018. doi: 10.1080/00288306.2018.1494006.

Peltzer, G., Crampé, F., Hensley, S., and Rosen, P. Transient strain accumulation and fault interaction in the Eastern California shear zone. *Geology*, 29(11):975, 2001. doi: 10.1130/0091-7613(2001)029<0975:tsaafi>2.0.co;2.

Reid, H. *The California Earthquake of April 18, 1906, Report of the State Earthquake Investigation Commission*. Carnegie Institution of Washington, Washington, D.C, 1910.

Reilinger, R., McClusky, S., Vernant, P., Lawrence, S., Ergintav, S., Cakmak, R., and Ozener, H. GPS constraints on continental deformation in the Africa-Arabia- Eurasia continental collision zone and implications for the dynamics of plate interactions. *Journal of geophysical research*, 111(B5), 2006. doi: 10.10292005JB004051.

Rockwell, T. K., Lindvall, S., Herzberg, M., Murbach, D., Dawson, T., and Berger, G. Paleoseismology of the Johnson Valley, Kickapoo, and Homestead Valley Faults: Clustering of Earthquakes in the Eastern California Shear Zone. *Bulletin of the Seismological Society of America*, 90(5):1200–1236, Oct. 2000. doi: 10.1785/0119990023.

Salisbury, J. B., Arrowsmith, J. R., Brown, N., Rockwell, T., Akciz, S., and Ludwig, L. G. The Age and Origin of Small Offsets at Van

Matre Ranch along the San Andreas Fault in the Carrizo Plain, California. *Bulletin of the Seismological Society of America*, 108 (2):639–653, Jan. 2018. doi: 10.1785/0120170162.

Scharer, K., Weldon, R., Biasi, G., Streig, A., and Fumal, T. Ground-rupturing earthquakes on the northern Big Bend of the San Andreas Fault, California, 800 A.D. to Present. *Journal of Geophysical Research: Solid Earth*, 122(3):2193–2218, Mar. 2017. doi: 10.1002/2016jb013606.

Shao, Y., Liu-Zeng, J., Van der Woerd, J., Klinger, Y., Oskin, M. E., Zhang, J., Wang, P., Wang, P., Wang, W., and Yao, W. Late Pleistocene slip rate of the central Haiyuan fault constrained from optically stimulated luminescence, 14C, and cosmogenic isotope dating and high-resolution topography. *GSA Bulletin*, 133 (7-8):1347–1369, Oct. 2020. doi: 10.1130/B35571.1.

Shen, Z.-K., Wang, M., Li, Y., Jackson, D. D., Yin, A., Dong, D., and Fang, P. Crustal deformation along the Altyn Tagh fault system, western China, from GPS. *Journal of Geophysical Research: Solid Earth*, 106(B12):30607–30621, 2001. doi: 10.1029/2001JB000349.

Shimazaki, K. and Nakata, T. Time-predictable recurrence model for large earthquakes. *Geophysical Research Letters*, 7(4): 279–282, Apr. 1980. doi: 10.1029/gl007i004p00279.

Sieh, K. E. and Jahns, R. Holocene activity of the San Andreas fault at Wallace Creek, California. *Geological Society of America Bulletin*, 95:883–896, 1984. doi: 10.1130/0016-7606(1984)95<883:HAOTSA>2.0.CO;2.

Sutherland, R., Berryman, K., and Norris, R. Quaternary slip rate and geomorphology of the Alpine fault: Implications for kinematics and seismic hazard in southwest New Zealand. *Geological Society of America Bulletin*, 118(3–4):464–474, Mar. 2006. doi: 10.1130/b25627.1.

Tong, X., Smith-Konter, B., and Sandwell, D. T. Is there a discrepancy between geological and geodetic slip rates along the San Andreas Fault System? *Journal of Geophysical Research: Solid Earth*, 119(3):2518–2538, Mar. 2014. doi: 10.1002/2013jb010765.

Ulrich, T., Gabriel, A.-A., Ampuero, J.-P., and Xu, W. Dynamic viability of the 2016 Mw 7.8 Kaikōura earthquake cascade on weak crustal faults. *Nature Communications*, 10(1), Mar. 2019. doi: 10.1038/s41467-019-09125-w.

Van Der Woerd, J., Tapponnier, P., J. Ryerson, F., Meriaux, A.-S., Meyer, B., Gaudemer, Y., Finkel, R. C., Caffee, M. W., Guoguan, Z., and Zhiqin, X. Uniform postglacial slip-rate along the central 600 km of the Kunlun Fault (Tibet), from 26Al, 10Be, and 14C dating of riser offsets, and climatic origin of the regional morphology. *Geophysical Journal International*, 148(3):356–388, Mar. 2002. doi: 10.1046/j.1365-246x.2002.01556.x.

van Dissen, R. Slip rate variations on major strike-slip faults in central New Zealand and potential impacts on hazard estimation, 2020. https://repo.nzsee.org.nz/handle/nzsee/1691.

Wallace, L. M., Barnes, P., Beavan, J., Dissen, R. V., Litchfield, N., Mountjoy, J., Langridge, R., Lamarche, G., and Pondard, N. The kinematics of a transition from subduction to strike-slip: An example from the central New Zealand plate boundary. *Journal of Geophysical Research: Solid Earth*, 117(B2), 2012. doi: https://-doi.org/10.1029/2011JB008640.

Wechsler, N., Rockwell, T. K., and Klinger, Y. Variable slip-rate and slip-per-event on a plate boundary fault: The Dead Sea fault in northern Israel. *Tectonophysics*, 722:210–226, Jan. 2018. doi: 10.1016/j.tecto.2017.10.017.

Weldon, R., Scharer, K., Fumal, T., and Biasi, G. Wrightwood and the earthquake cycle: What a long recurrence record tells us about how faults work. *GSA Today*, 14(9):4, 2004. doi: 10.1130/1052-5173(2004)014<4:watecw>2.0.co;2.

Weldon, R. J. and Sieh, K. E. Holocene rate of slip and tenta-tive recurrence interval for large earthquakes on the San Andreas fault, Cajon Pass, southern California. *Geological Society of America Bulletin*, 96(6):793, 1985. doi: 10.1130/0016-7606(1985)96<793:hrosat>2.0.co;2.

Yönlü, O. and Karabacak, V. Surface rupture history and 18⊠kyr long slip rate along the Pazarcık segment of the East Anatolian Fault. *Journal of the Geological Society*, 181(1), Dec. 2023. doi: 10.1144/jgs2023-056.

Zhang, P.-Z., Molnar, P., and Xu, X. Late Quaternary and present-day rates of slip along the Altyn Tagh Fault, northern margin of the Tibetan Plateau. *Tectonics*, 26(5), 2007. doi: 10.1029/2006TC002014.

Zhao, D., Qu, C., Bürgmann, R., Gong, W., Shan, X., Qiao, X., Zhao, L., Chen, H., and Liu, L. Large-Scale Crustal Deformation, Slip-Rate Variation, and Strain Distribution Along the Kunlun Fault (Tibet) From Sentinel-1 InSAR Observations (2015–2020). *Journal of Geophysical Research: Solid Earth*, 127 (1):e2021JB022892, 2022. doi: 10.1029/2021JB022892.

Zinke, R., Dolan, J. F., Rhodes, E. J., Van Dissen, R., and McGuire, C. P. Highly Variable Latest Pleistocene-Holocene Incremental Slip Rates on the Awatere Fault at Saxton River, South Island, New Zealand, Revealed by Lidar Mapping and Luminescence Dating. *Geophysical Research Letters*, 44(22), Nov. 2017. doi: 10.1002/2017gl075048.

Zinke, R., Dolan, J. F., Rhodes, E. J., Van Dissen, R., McGuire, C. P., Hatem, A. E., Brown, N. D., and Langridge, R. M. Multimillennial Incremental Slip Rate Variability of the Clarence Fault at the Tophouse Road Site, Marlborough Fault System, New Zealand. *Geophysical Research Letters*, 46(2):717–725, Jan. 2019. doi: 10.1029/2018gl080688.

Zinke, R., Dolan, J. F., Rhodes, E. J., Van Dissen, R. J., Hatem, A. E., McGuire, C. P., Brown, N. D., and Grenader, J. R. Latest Pleistocene–Holocene Incremental Slip Rates of the Wairau Fault: Implications for Long-Distance and Long-Term Coordination of Faulting Between North and South Island, New Zealand. *Geochemistry, Geophysics, Geosystems*, 22(9), Sept. 2021. doi: 10.1029/2021gc009656.